Unione Europea

PON Ricerca e Innovazione 2014- 2020

Ministero dell'Istruzione, dell'Università e della Ricerca

Dottorato di Ricerca in Ingegneria dei Prodotti e dei Processi Industriali

SCUOLA POLITECNICA E DELLE SCIENZE DI BASE

Dipartimento di Ingegneria Chimica, dei Materiali e della Produzione Industriale

TESI DI DOTTORATO DI RICERCA

XXX CICLO

PHYSICAL STABILITY OF STRUCTURED FLUIDS CONTAINING AIR BUBBLES

Comitato scientifico

Prof. Nino Grizzuti
Prof.ssa Rossana Pasquino
Ing. Vincenzo Guida
Dott. Fabio Zonfrilli

Candidata

Ing. Shadi Mirzaagha

Anno Accademico 2016/2017

Table of contents

Figures

Tables

INTRODUCTION

This PhD Research Project is developed in the framework of a collaboration between the "University of Naples Federico II" (Naples, Italy) and the "Procter and Gamble" company (P&G, Brussels Innovation Center, Belgium).

Special attention has been paid over the years to structured detergents due to their large application in everyday life. The essential components for the majority of these systems are surfactants, although final products usually have a complicated formulation including auxiliary components such as builders, water softeners, enzymes, brighteners, fragrances, foaming controllers, pigments etc.

The peculiarity of these detergents is to contain a structurant component capable to produce a permanent elastic microstructure to prevent settling of colloidal suspended particles and, therefore, to increase the product shelf-life.

Rheological studies on complex fluids, which mimic the detergence products, could have a key-role in designing physically stable products. In this Phd project, a simplified model of structured Heavy Duty Liquid, a liquid detergent for washing machines, is proposed. All auxiliary components of detergent systems are omitted from the formulation, so that the proposed model can be schematically described as a background surfactant solution reinforced by hydrophobic fibers. These fibers are added to the detergents to provide the desired rheological properties and specifically to provide a system with a yield stress and hence the ability of suspending objects like pigments, fragrances, silicone oil droplets or silicone microcapsules.

In spite of the many advantages assured by the presence of the fibers in terms of shelf life, the resulting system can be mechanically unstable. Basically, the main responsible for this instability is the load applied by air bubbles, which are generated during the processing stages and core. The fiber concentration, which dictates the yield stress of the fluid, aeration level and temperature can influence the stability of the final product. In particular, under given conditions, bubbles can apply a remarkable load on the fiber network during their buoyancy-driven rise, thus inducing the

collapse of the structure. The result is a clear phase separation, with the matrix without fibers standing on the bottom of the fluid volume, and a more concentrated system moving towards the free surface.

In this work various samples at different fiber concentration are studied. The rheological measurements at 20°C in dynamic and in steady modes have been conducted in a way to determine the dependence of the rheological parameters on the fiber content. As the HCO content is increased, the elastic response increases and a plateau modulus at low frequency appears, indicating the fingerprint of a gel-like network. Steady measurements confirm this response, by showing a yield stress at low shear rate values.
A time lapse photography technique has been used to monitor the time evolution of the air bubbles trapped in the fluids. The motion of single bubbles of different sizes in lowly aerated fluids are tracked to obtain their terminal velocity. Data have been collected, critically analyzed and compared with theoretical predictions and a simulation model made by Comsol Multiphysics software.

At last, the air bubble effect on physical stability of structured and highly aerated fluids is studied at different temperatures (25-30-40-50°C). The instability splitting edge has been measured as function of time and the instability has been determined by two parameters: the applied load (aeration and spheres size) and the fluid rheology (yield stress).

The remaining of the work is organized as follows. In Section 1 a literature review concerning the rheological studies on yield stress fluids, on the rising motion of spherical objects and on the collapse and flocculation failure has been carried out. In Section 2 a description of the materials and the methods used in the current Phd project is given. From Section 3 to 5, the Phd results are properly discussed. Finally, concluding remarks and future developments are given in Section 6.

Chapter I

1. State of the art

Home-care products are detergent systems that differ for applications, formulation and structure. From a physical point of view, detergents are usually suspensions where a surfactant-based, micellar solution represents the continuous phase and colloidal fibers are added in order to provide viscoelasticity to the matrix. Basically, the system can be mechanically unstable, if the air bubbles, which are included during the making and packaging processes, apply a remarkable load on the fiber network.

Academic and product-oriented researchers are interested in understanding the failure dynamics and, ultimately, in obtaining predictions on the physical stability of structured fluids over ageing. In the first chapter the state of art, pertaining to the subject of this thesis, is presented. In particular, it focuses on the rheological behavior of the structured fluid, on the motion of the single spherical body in a yield stress fluid and on the origins of the delayed collapse.

1.1. Yield stress fluid

The fluid used for our experiments is a surfactant micellar solution, in which colloidal fibers are added. In presence of attractive interactions, these colloidal particles can aggregate into ramified, fractal cluster, whose density decreases as their size increases. As a result, they can, in principle, grow to form a space-spanning network, or a gel, at arbitrarily low volume fraction φ. The network formed through colloidal aggregation is the most relevant feature controlling the rheological properties of such complex materials. The fiber network is the main responsible of the solid-like behavior and the resulting fluid, reinforced with the fibers, is characterized by a yield stress. The yield stress is the critical shear stress that must be exceeded before irreversible deformation and flow occur. Viscoelastic materials are often characterized by a yield stress. Once the yield stress is exceeded, the material exhibits viscous liquid behavior. For applied stresses below the yield stress, the material deforms as an elastic body. An elastic material is deformed under stress, but then

returns to its original shape when the stress is removed. One method that has been frequently used for characterizing yield stress materials is to define two yield stresses—one static and one dynamic—or even a whole range for the yield stress (Mujumdar *et al.*, 2002). The static yield stress is defined as the stress at which flow is initiated, while the dynamic yield stress is an extrapolation to zero shear rate of the stress applied to keep the sample flowing and is generally lower than the static value. Despite the yield stress clearly controls the behavior of many materials, even in daily activities such as squeezing a toothpaste from a tube or dispensing ketchup from a bottle, the concept of a true yield stress is still a topic of much debate (Barnes and Walters, 1985; Spaans *et al.*, 1995). According to Barnes and Walters all materials can creep or flow in a similar manner over long enough timescales and consequently many materials, which are considered to have a true yield stress, are actually very high viscosity liquids. For this reason, the term apparent yield stress is widely used and is considered to represent the critical stress at which there is a distinct drop in viscosity. This key characteristic can be depicted in Figure 1.1 with a material having a true yield stress showing an infinite viscosity approaching zero shear rate and a material with an apparent yield stress showing a zero shear viscosity plateau. The distinction really needs to be made at low shear rates (representing long times) since, within a more limited shear rate range, the material may appear to have a yield stress, but at much lower shear rates a zero shear viscosity plateau can be observed.

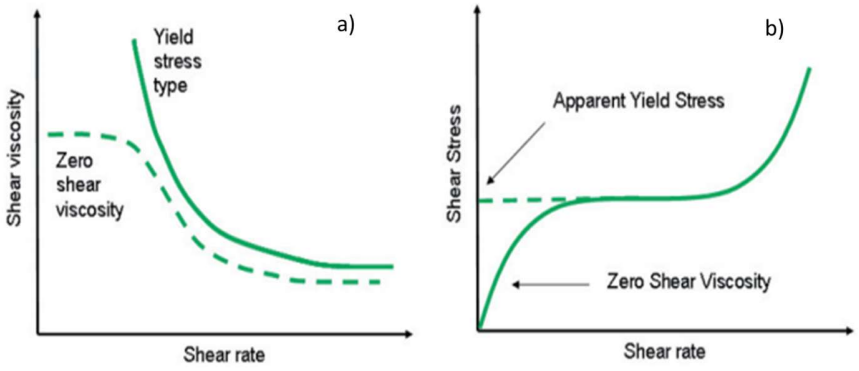

Figure 1.1*: Flow curve for a material with a true yield stress and a zero shear viscosity: a) viscosity versus shear rate b) shear stress versus shear rate.*

The determination of a yield stress as a true material constant can be difficult as the measured value can be very much dependent on the measurement technique employed and the conditions of the test.

One such variable, which can affect the measured yield stress value, is time.

"The magnitude of any measured yield stress depends on the time of the measurement", because viscoelastic and thixotropic effects can mask other features, in fact "the measurement of the yield stress... is the measure of the experimenter's patience" (Chan Man Fong and De Kee, 1993).

"Suppose one works with Ph.D. chemical engineering students, so that the time scale is expanded to three years; and at the same time one finds a system where the density difference is 0.015 g/cm^3. …Yield stress is the ratio of the system density difference to the patience of the graduate student." (Astarita, 1990).

James (1987) demonstrated that a variation in the yield stress by more than one order of magnitude can be obtained depending on how it is measured. To determine the duration of the observation/experiment vs. a characteristic time of the material deformation, Reiner (1964) defines the Deborah number as *Equation (1.1).*

$$De = \frac{t_r}{t_{obs}} \qquad \textbf{(1.1)}$$

where t_r is a characteristic relaxation time and t_{obs} the duration of the observation/experiment. *De* is zero for a Newtonian fluid and is infinite for a solid. The yield stress is directly related to the Deborah number.

The timescale or frequency of testing is also important since viscoelastic materials may respond differently depending on the relaxation behavior of the material and the rate of deformation (Spaans and Williams, 1995). Micro-structural relaxation processes are best evaluated using dynamic testing on a rotational rheometer with inverse frequency correlating with time. Some typical frequency spectra and their mechanical analogues are shown in *Figure 1.2*. Since G' is the modulus related to elasticity (and association) then, when its value exceeds the viscous modulus (G"), which is related to flow, the material can be considered to have an associated structure and hence a yield

stress. For a material to have a true yield stress then G' must exceed G" at infinitely low frequencies, which would be the case for a viscoelastic solid and an ideal gel. For a viscoelastic liquid the material will only appear to yield in the frequency range where G' exceeds G" and thus these materials can be considered to have an apparent yield stress or critical stress. It is not uncommon for real materials to show elements of all these types of behavior over a wide frequency range. However, due to measurement and time constraints it is often only possible to observe a limited frequency range.

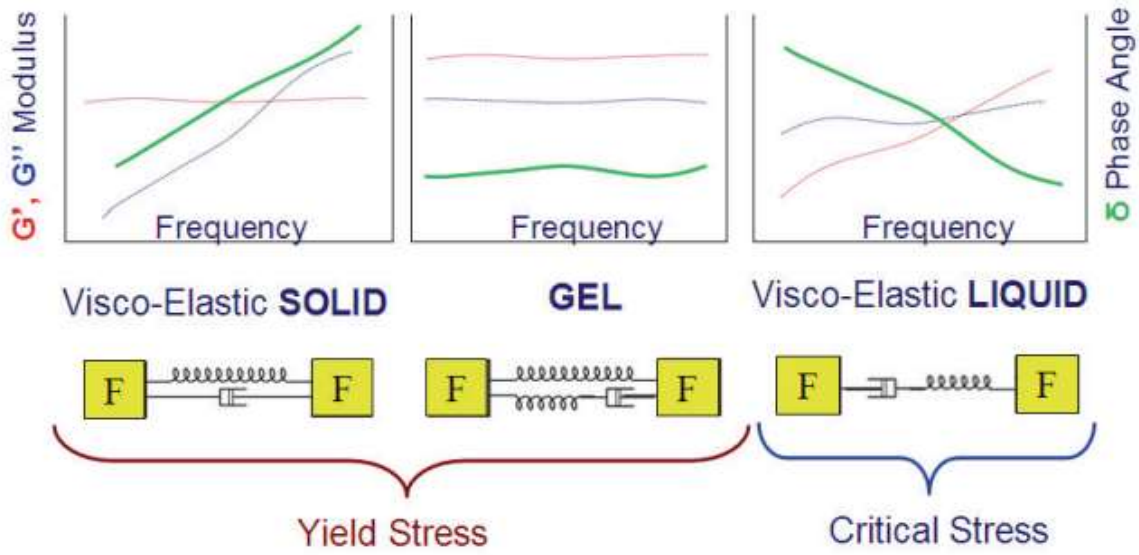

Figure 1.2: *Illustration showing some typical frequency profiles for materials with a yield stress/critical stress and their mechanical analogues*

Another important factor is temperature. At higher temperatures, material components have more thermal energy and, hence, a lower stress input is required to initiate flow. Consequently, the yield stress tends to decrease with increasing temperature as long as there is no thermally induced structural enhancement at elevated temperatures (Larson, 1999).

1.2. Rheology and microstructure properties of suspensions

In the last decades special attention has been paid to structured detergents, due to their wide range of applications in everyday life (Zana and Kaler, 2007; Kuo-Yann Lai, 2015). From a physical point of view, most detergents are based on aqueous solutions of surfactants, with fibers usually added to improve the final mechanical properties. Very different micellar structures can be obtained by changing the surfactant concentration or the temperature and the pH (Larson, 1999). The different geometries of the micelles (such as spherical micelles, vesicles, lamellar bilayers etc.) are described by the packing factor parameter (Israelachvili *et al.*, 1976). The transition from one morphology to another, also with very small variations in composition and temperature, has many consequences on the macroscopic behavior of the solution (Gaudino *et al.,* 2015), and can in turn generate dramatic changes in the rheological response, making the surfactant systems suitable for different applications (Kefi *et al.*, 2004; Pasquino *et al.*, 2016).

When colloidal particles are suspended in a surfactant solution the microstructure can become even more complicated. The network, kept together by colloidal aggregation forces, is decisive to control the rheological properties of such complex materials. For the above reasons, a full understanding of the developing microstructure and of its stability is highly desired (Manley S. *et al.,* 2005).

Colloidal particles can have different shapes, such as spherical, ellipsoids, rods, and different sizes. In the specific case of rigid rod suspensions, their fluid-phase micro dynamics, rheology and microstructure have been investigated in a number of contexts (Larson, 1999 ; Berry, 1987; Dhont and Briels, 2003; Pryamitsyn and Ganesan, 2008; Russo, 1993; Berry, 1987; Sherwood, 1981; Savenko and Dijkstra, 2006; Petrie, 1999; Powell, 1991; Rahnama *et al.*, 1995; Stover *et al.*, 1992; Mukhijaa and Solomon, 2011; Hong *et al.*, 2006; Solomon and Spicer, 2010; Barnes, 2000). Four key properties control the microstructure and rheology of rod suspensions: particle number density, aspect ratio, flexibility and interparticle forces. The number density ρ is proportional to the rod volume fraction $\phi = \rho V_p$ where V_p is the rod particle volume. It is possible to define three concentration regimes (Doi and Edward, 1986). For $\rho << 1/L^3$, where L is the rod length, the rods are dilute and contacts are occasional. In the semi-dilute range, $1/L^3 << \rho << 1/bL^2$, where b is the rod width, each rod still has rather few structural interactions with its neighbors and the Brownian rotational motion is not negligible. Finally, in the concentrated regime, $\rho >> 1/bL^2$, rod rotation is

severely hindered by strong structural correlations and multiple, random inter-rod contacts. The aspect ratio has also a fundamental role in the amorphous packing and phase stability of rods in suspensions. Indeed, Brownian translational and rotational dynamics are a strong function of the rod length (Doi and Edward, 1986). In this case, it is the ratio of rod length, *L*, and width, *b*, which is defined as the aspect ratio *L/b*, that determines the effect of excluded volume interactions on the microstructure. At high aspect ratios, rod glasses may form due to caging and packing constraints at seemingly low-volume fractions. At low aspect ratio rod gels are formed. The progression from glass to gel in rods can be generated through different combinations of volume fraction and aspect ratio. Therefore, the dynamical transition can vary from bonded gels (with heterogeneous fractal structure) to caged glasses (with homogeneous amorphous structure) (Huang *et al.*, 2006, Zhang *et al.,* 2009; Wilkins *et al.*, 2009; Krall and Weitz, 1998; Mohraz *et al.*, 2006; Brinke *et al.*, 2007).The rods may also be either fully rigid or flexible. The flexibility is measured as L/l_p, where l_p is the persistence length. For rigid rods $L/l_p<<1$, while for semi-flexible filaments $L/l_p\sim1$. The role of the persistence length and the consequent rod flexibility on the rheological response of the systems is still under debate (Tassieri, 2017). Regarding interparticle forces, rod contacts may involve charges, dispersions, friction interaction and/or depletion forces (Chen and Schweizer, 2002). In fiber/surfactant systems, as the one studied in the present work, when particles come close to each other surfactant micelles are excluded from the tiny interparticle space. The resulting surfactant-depleted region leads to a local difference in osmotic pressure. The overall effect is that the two adjacent particles producing the small gap are pulled together. This pulling force can be strong enough to overcome any repulsive forces and, with the addition of the van-der-Waals force, it can produce flocculation of the particles. This effect, known as depletion flocculation, can also be caused by very small particles present in the dispersion. When the volume concentration of micelles exceeds a critical value the onset of depletion flocculation occurs. At the beginning of flocculation, where the energy of interaction is relatively small, the particles will be able to approach closely in a floc. However, with increase in flocculation, the energy of attraction becomes larger and a more open floc structure can be obtained (Packman and Tadros, 1992). Another important manifestation of the depletion interaction is the formation of structural forces due to free energy changes upon packing of macromolecules in the confined space between approaching surfaces. Experimental and theoretical works (Sober and Walz, 1995) on depletion interactions have suggested the behavior of

a longer range repulsive potential energy barrier with increasing macromolecule concentration. This repulsive barrier has been explained in terms of interactions among the macromolecules as they are forced into the confining region between particles.

From a macroscopic point of view, as previously explained, colloidal systems of the type investigated in this work can often show a mechanical gel-like behavior. To determinate the structure of a gel from rheological measurements, different scaling methods are proposed. (Brown and Ball, 1985; Brown, 1987; Ball, 1989)

Brown and Ball (1985) were the first to develop a scaling theory on the elastic behavior of the gel structure. Shii *et al*. (1990) extended these data and developed a new scaling model, including previous results (Buscal *et al*., 1988; Kantor and Webman, 1891). They observed an attractive fractal gel of spheres, which in principle should not have a critical gelation limit. In this model, they assumed two different gel-like regimes: a strong-link regime at low particle concentrations, where the elasticity of the gel is given by the intrafloc links; and a weak-link regime at high particle concentrations, where the flocs are more rigid and the elasticity of the interfloc links determines the gel elasticity. The two regimes are extreme situations. Wu and Morbidelli (2001) developed a new scaling model to relate the microstructure of colloidal gels to their macroscopic elastic proprieties and introduced an intermediate regime where both inter and intrafloc links contribute to the elasticity of the gel. In these three regimes, the elastic modulus often follows a power law dependence upon fibril weight concentration, $G_0 \sim C^{\alpha}$ (Pa¨a¨kko¨ *et al.*, 2007; Tatsumi *et al.*, 2002; Rezayati Charani *et al.*, 2013; Saito *et al.*, 2011) at least in the case where the dynamic moduli are almost independent on the angular frequency and are evaluated at a fixed frequency. The magnitude of the exponent α can be different, due to the type of fibrils and solvent quality (Quennouz *et al.*, 2016). For example, the power index of cacao butter, milk fat and tallow, examples of other weak-link regime systems, are 1.67, 1.01, and 1.72, respectively (Morbidelli, 2001). In the strong-link regime, a larger power law exponent is usually expected, i.e. $\alpha = 2.25$ for fibrillated cellulose fibers (Naderi *et al.,* 2014) and $\alpha \sim 4$ for boehmite alumina gel (Shii *et al.*, 1990). The most extensive studies of the elastic scaling behavior of colloidal gels made by fibers refers to nanofibrillated cellulose (NFC). Quennouz *et al.* have reported the rheological proprieties of cellulose nanofibrils in different surfactant solution. The fluids display a gel like behavior due to the associative

thickening mechanism resulting from the bridging between the fibers through micelles. This results in a strong shear thinning behavior and a power- law dependence of the elastic modulus on concentration, $G_0 \sim C^{2.1}$. Naderi *et al.* (2014) demonstrated that when nanofibrillated cellulose (NFC) is carboxymethylated, it shows properties similar to other NFC systems available in literature. The storage modulus scale with concentration with a power law index of 2.4, slightly higher than the theoretical value of 2.25, proposed by de Gennes (1979) and Doi and Edwards (1978) for polymer systems in a semidilute regime. This suggests that the repulsive character of the fibers and their entanglements could induce system gelation.

In absence of surfactant molecules, Tatsumi *et al.* (2002) studied various NFC suspensions in a wide range of fiber length and diameter and found that, also in this case, the fluid shows a gel like behavior with an elastic plateau modulus and a yield stress value dependent on the concentration of fibers with a power law index of 9/4. This suggests that α does not reflect the individual characteristics of the fibers but the structural properties of the suspensions. The power of 9/4 is consistent with the scaling theory of polymer gels in a good solvent.

Many researchers consider the fluid yield stress as a necessary condition for the presence of a fiber network. For example, Kerekes *et al.* (1985) summarized this behavior with an empirical power law equation: $\sigma_0 = kC^{\alpha}$ where σ_0 is the yield stress of the suspension and k and α are constants. The latter are unique for each suspension, with values in the range $1.18 < k < 24.5$ and $1.26 < \alpha < 3.02$. From the above discussion, it can be concluded that the rheological behavior of fibril-based colloidal systems displays a wide range of possible responses that depend on many different factors.

One of the aims of this work is to better understand the rheological response of a system formed by Hydrogenated Castor Oil (HCO) fibers suspended in a water surfactant solution, based on a surfactant widely used in commercial products. HCO can crystallize in three different morphologies: fiber, rosette and irregular crystals (Yang and Hrymak, 2013; De Meirleir *et al*., 2014), depending on temperature, shear rate and time. Yang *et al.* (2013) have investigated the effect of HCO crystal morphology on their rheological response in aqueous suspensions. A power-law index of 1.5 has been found between yield stress and particle volume concentration, regardless

of the irregular crystal morphology. Also De Merleier *et al.* (2014) have studied the morphology and the rheological behavior of the HCO systems, at concentrations ranging from 0.08 to 3wt%. The most interesting crystal shape is given by thin fibers because they tend to form an entangled network. The HCO-fiber systems are produced by controlling the crystallization rate of HCO in LAS aqueous medium neutralized with Monoethylamine (MEA). The power law exponents of the elastic plateau modulus on the HCO concentration depends on the morphology. More specifically, for fibrous systems the slope is dependent on concentration and two values for the power law indices are measured, 1.52 and 0.94, in different concentration ranges.

1.3. The rising motion of single bubble in a yield stress fluid

The motion of a spherical body through a complex fluid can be considered as a benchmark problem that provides information about the rheological characteristics of the fluid and the flow field around the particle. This topic is also relevant in many industrial applications, such as biochemical, food and detergent processing. For example, in the manufacturing and bottle filling processing stages, the presence of non-rising bubbles may be unwelcome and can induce instabilities (Clift *et al.*, 1978; Putz *et al.*, 2008; Ansley *et al.*, 1967; Gueslin *et al.*, 2006). The buoyancy driven motion of an air bubble in a Newtonian fluid has been extensively investigated both theoretically and experimentally (Harper, 1972; Clift *et al.*, 1978; Magnaudet and Eames, 2000; Tsamopoulos *et al.*, 2008). When the suspending fluid becomes non-Newtonian, however, the rising motion may be complicated. A wide body of literature considers the motion of bubbles in a viscoplastic material characterized by a yield stress and deals with the relative role of their size. Sufficiently small bubbles, such that the load exerted on the fluid does not overcome the yield stress, may remain entrapped into the liquid, without any motion (Bhavaraju *et al.*, 1978; Dubash and Frigaard, 2004; Dubash and Frigaard, 2007). In the mid '60s Astarita and Apuzzo (1965) investigated the bubble shapes and the terminal velocities in Carbopol solutions at different concentrations. They observed a jump in the rising velocity as a function of the bubble volume that depends on the yield stress of the material. Several theoretical and numerical works confirmed Astarita and Apuzzo's observations on the existence of a critical bubble radius to achieve motion (Dubash and Frigaard,

2007; Dimakopoulos *et al.*, 2013; Fraggedakis *et al.*, 2016). The bubble dynamics become even more complicated when a surfactant solution is considered. The effects of surfactant type on bubble surface and the resulting viscous friction have been extensively studied (Denkov *et al.*, 2005; Tcholakova *et al.*, 2008). The same qualitative dynamics are encountered by a solid sphere sedimenting or rising in a viscoplastic fluid, according to the density difference (Fraggedakis *et al.*, 2016; Beris *et al.*, 1985). Also in this case, the buoyancy force has to overcome the yield stress of the fluid to allow the particle to move. Nevertheless, there are relevant differences between bubbles and solid spheres which can be summarized in two main points:

- bubbles can undergo surface deformation during their rising motion, more or less pronounced depending on their size and the rheological properties of the fluid;

- the boundary condition at the interface is different, slip condition for the bubble and no-slip for the solid sphere.

Beris *et al.* (1985) numerically investigated the conditions such that a particle does not move in a Bingham fluid. They defined the dimensionless yield ratio as *Equation (1.2)*:

$$Y_c = \frac{3\sigma_0}{2(\rho_l - \rho_b)gD} \qquad \textbf{(1.2)}$$

where σ_0 is the yield stress of the fluid, ρ_b and ρ_l are the particle and the fluid densities, respectively, g is the gravitational acceleration, D is the particle diameter. Yc represents the ratio between the yield stress of the fluid and the characteristic stress exerted by the particle. In other words, it measures the strength of the creep applied by the sphere during its rising motion on the surrounding fluid compared to the yield stress characteristic of the fluid.

Beris et al. (1985) theoretically showed that a rigid sphere would not move if Y_c exceeds a critical value, $Y_{c,cr}$,= 0.072 (using Y_c as in *Equation (1.2)*, as for all the critical values shown in the following). From an experimental point of view, it is difficult to obtain accurate data sets when approaching $Y_{c,cr.}$ This is due, mainly, to the very low sphere velocity and to the consequent long

experimental time. Experimental data are, indeed, scarce and limited. The most extensive data set in literature is from Tabuteau *et al.* (2006) on Carbopol gels using ping-pong and metal spheres. They confirmed the theoretical predictions by Beris *et al.* (1985), extending the data set of Atapattu *et al.* (1995). Emady *et al.* (2013) experimentally determined a range of $Y_{c,cr}$ between 0.05 and 0.3 for different classes of suspending liquids. More specifically, they focused on cellulose microfibers suspensions and compared the obtained experimental data with the more classical Carbopol solutions, suggesting that the knowledge of the bulk yield stress is often not sufficient for a prediction of the motion/no motion of spherical bodies. They found, indeed, that the $Y_{c,cr}$ depends on the suspending fluid microstructure and can vary significantly: $Y_{c,cr}$ is much lower in the case of cellulose microfibers suspensions, if compared with Carbopol solutions. In addition, $Y_{c,cr}$ is different for bubbles and solid spheres, because of the possibility of deforming the bubbles and the different boundary condition, as explained before. For asymmetric bubbles, the $Y_{c,cr}$ can change significantly if compared to the value of 0.072, previously discussed for a solid sphere. For asymmetric bubbles Dubash and Frigaard (2004, 2007) found a value of $Y_{c,cr}$ four to ten times larger than the value $Y_{c,cr}$=0.25 found experimentally by Sikorski *et al.*. (2009). For spherical bubbles, N. Dubash, and I.A. Frigaard (2004) obtained a value of $Y_{c,cr}$=0.43, whereas Tsamopolous *et al.*(2008) found a value of 0.10 for bubbles rising in a Bingham fluid. de Bruyn (2004; 2006) studied the velocity dependence of the drag force on a sphere moving through a foam, and Chafe and de Bruyn (2005) through Bentonite clay suspensions. Jossic and Magnin (2001) and Merkak *et al.* (2006) investigated the evolution of the velocity of spheres in response to an applied force. They observed the effect of roughness of the sphere's surface: the drag force was about 25% higher for rough spheres as compared to smooth spheres.

The problem of a yield-stress fluid flow past solid objects has been also extensively investigated through numerical simulations (Balmforth *et al.*, 2014; Mitsoulis and Tsamopoulos, 2017; Saramito and Wachs, 2017). Following the aforementioned work by Beris *et al.* (1985), the problem of the flow around a solid sphere has been revisited by Blackery and Mitsoulis (1997) for a Bingham model and by Beaulne and Mitsoulis (1997) for a Herschel-Bulkley constitutive equation. The simulation results by Blackery and Mitsoulis (1997), obtained by "regularizing" the discontinuous Bingham model (Papanastasiou, 1987), closely matched those from Beris *et al.*

(1985) both in terms of drag coefficient and shape of yielded/unyielded region. The effect of confining walls was also investigated. A similar analysis has been carried out for different shapes of rising/sedimenting bodies (Roquet and Saramito, 2003; Mitsoulis, 2004; Mitsoulis and Galazoulas, 2009), for two spheres translating collinearly (Liu *et al.*, 2003; Yu and Wachs, 2007, Derksen, 2011), by including the effects of inertia (Yu and Wachs, 2007, Derksen, 2011), slip conditions at the fluid-particle surface (Deglo de Besses *et al.*, 2003), and elasticity (Fraggedakis *et al.*, 2016). It is clear from the above experimental and numerical results both on solid spheres and bubbles that the $Y_{c,cr}$ is never unity because the particle must yield a finite volume of fluid to move. This point can be rephrased in terms of an effective particle volume, as the particle "feels" a volume of fluid that is larger than its own volume, whereas the fluid further away from the spheres remains unyielded. As a consequence, a spherical particle immersed in a fluid with yield stress moves when its load overcomes a multiple of the fluid yield stress given by $1/Y_{c,cr}$. The latter, therefore, can be also seen as a dimensionless critical particle diameter below which, for a given yield stress, no motion takes place in a reasonable experimental time window. The presence of different and contradictory values of $Y_{c,cr}$ for various systems reported in the literature points, on the one hand, to the difficulty to carry out consistent and reproducible experiments. On the other hand, it suggests that the motion of an object in a yield stress fluid is still an open issue.

As far as experimental difficulties are concerned, various factors must be considered: 1) the ability to univocally measure the macroscopic yield stress of the fluid; 2) the effort to obtain isolated bubbles trajectories, which can be biased by many different phenomena, e.g., ripening, desorption/absorption, bubble/bubble hydrodynamic interactions; 3) the presence of mechanical disturbances (such as vibrations and instrumental creep) and optical errors (refractions) in the experimental setup; iv) the often long duration of experiments, when small bubbles and fluids with a high yield stress are considered.

In this work, air bubbles are small and undeformable, as proven by the low values of the capillary number. Bubbles and solid spheres, therefore, will be treated in the same way, the only difference standing in the boundary conditions used for the simulations. It is important to highlight that much of the previous experimental work on yield-stress fluids has been done using Carbopol solutions,

whereas in our case the yield stress comes from the presence of colloidal fibers in the surfactant solution.

1.4. Collapse and flocculation of structured fluid

Despite the practical importance of suspensions of colloidal particles, they still present many unclear issues (Teece et al., 2014). Thanks to the attractive interactions, the colloidal system can aggregate into ramified, fractal clusters, whose density decreases as their size increases. As a result, they can, in principle, grow to form a space-spanning network, or gel, at arbitrarily low volume fractions ϕ (Manley et al. 2005). This arrangement of colloids is not stable and the gel suddenly destabilizes after some finite time.

The properties of particulate gels depend of the strength of the inter particle bonds. It is helpful to distinguish between strong and weak gels, as already outlined in Section 1.2. In the strong gel the thermal flocculation does not play a role on the inter-particle bonds. Rather, the gel shows a sedimentation behavior. In contrast, the inter particle interactions in the weak gel regime have a finite lifetime due to thermal flocculation. Weak gels have a more complex behavior and it is possible to distinguish two effect of the bond-breaking flocculation: creeping sedimentation and delayed collapse. The first phenomenon occurs in distinct stages, characterized by a slow initial compression, after which gels undergo significant restructuring and rapid sedimentation, followed by a slow final compression to an equilibrium height. Alternatively, the delayed collapse can occur smoothly, so the rate decreases with time. (Buscall *et al.*, 2009; Manley *et al*., 2005). Delayed collapse has been observed in many system (Glasrud *et al.,*1993; Parker et al.,1995; Allain *et al.,*1995; Poon *et al.*,1999; Verhaegh *et al.*,1999; Starrs *et al.,*2002; Kilfoil *et al.*,2003; Derec *et al.,*2003; Blijdenstein *et al.*,2004; Gopala *et al.,*2006; Huh *et al.,*2007; Kamp *et al.,*2009; Bartlett *et al.,*2012) and can be considered a universal feature of weak gels.

When the network is locally affected by particle sedimentation/aggregation, a flocculation instability effect occurs. A floc is a collection of particles where the concentration decreases from

the center towards the outside, due to the way flocs are formed (Barnes, 2000). The simplest way of describing such a floc is to use fractals; in this way, we are able to depict the concentration falling off from the floc center, which usually follows a power law like in *Equation (1.3)*

$$\beta = \left(\frac{R_0}{a}\right)^m \qquad \textbf{(1.3)}$$

where β is the number of particle in a floc, a is the radius of the particles, R_0 is the radius of the smallest sphere enclosing the floc and m is the fractal dimension. m can vary from almost 3 for the densest floc to about 1 for a very open 'linear' floc with a few radiating arms. Ultimately, the value of m depends on the magnitude of particle interaction forces (Barnes, 2000). Floc formation can be induced by adding an electrolyte to the suspension or by changing the surface charge altering the pH (Larson, 1999). Flow can also affect flocculation: strong shearing can result in the flocs being reduced to the primary particles, but shearing at a low shear rate results in the partial breakdown or reformation of flocs.

Up to now we have discussed the collapse of colloidal gels, mainly due to interparticle forces. When other entities are added to the colloidal gels, such as spherical bodies (solid spheres or gas bubbles) the collapse can also be induced due to interaction between these entities and the gel itself. Few examples are reported in literature, regarding systems as ethylene glycol distearate (Caggioni, 2012) and HCO fiber suspensions (Zanchetta *et al.,* 2013), where glass-beads are used to induce the instability. Other investigated systems encompass colloidal gels obtained by salt induced destabilization of silica particles and gels obtained by inducing depletion interactions between colloids or emulsion droplets (Kamp and Kilfoil, 2009).

Despite this wide variety of systems, the basic features of the sample evolution are essentially the same: after a delay or initial compression period, the gel catastrophically collapses and eventually consolidates at a final equilibrium height.

1.5. Theory of Poroelasticity

Our system made by HCO fibers in aqueous surfactant solutions is nearly perfectly buoyancy - matched, such that HCO/surfactant systems are usually homogeneous and stable for years. However, when loaded with buoyancy - mismatched particles, two distinct scenarios can be observed. Due to the total particle load applied during the rising motion of spherical bodies, the HCO-network can be slowly compressed and then can eventually collapse after a delay time. These processes lead to the visual appearance of two distinct phases: a clear HCO-free phase and a turbid phase that contains the HCO-fibers and the particles. The fiber and particle distributions remains rather homogeneous in the turbid phase during the entire compression and collapse process.

Because of the visual distinction between the two phases one can assess such failure mode by simply monitoring the time-evolution of the moving interface between both phases.

The route generally chosen for the description of this process is the poro-elastic model, which we briefly outline in the following section.

Since the seminal papers by Biot (1941) and by Buscall and White (1987) , it has been recognized that the gravitational collapse of colloidal gels can be generally understood within the framework of the poro-elastic model. Under the effect of gravitational stress, the gel behaves like a porous medium that is squeezed like a sponge. This forces the background fluid to flow through the pores of the gel. As gels compress, a sharp interface appears between the highly turbid gel and the clear solvent: indeed, gels must expel the background solution in order to compress. The macroscopic behavior of the fluid can be studied by tracing the time evolution of the height interface.

The collapse of colloidal gels results from a balance between the gravitational load, the resistance to fluid flow, and the systen elastic and plastic properties. Their stability and collapse behavior under gravity can be predicted by the theory of poroelasticity (Biot, 1941).

Manley *et al*. (2005) presented a model for the collapse stage based on the Theory of Poroelasticity (Biot, 1941). The model takes into account the resistance to compression arising from a combination of the fluid pressure and the elasticity of the network. For weakly elastic gels, the

theory captures the initial compression and can be used to describe the behavior of the gel up to the delayed failure time, t_d, after which the rapid collapse is observed. The mechanism governing the initial stage is assumed to be the backflow of the fluid through the porous network, which determines the initial rate of compression, v_0. Furthermore, it has been observed that v_0 is nearly constant. The interstitial fluid, which is the surfactant background solution of the gel, is subjected to a pressure P due to the weight of the gel; thus, it flows at a velocity v, within the porous and deformable network, leading to a local displacement of the solid $w(z,t)$ in the z direction. Using Darcy's Law:

$$(\mathbf{1}-\boldsymbol{\phi})\left(\boldsymbol{v}-\frac{\partial \boldsymbol{w}}{\partial \boldsymbol{t}}\right)=-\frac{\boldsymbol{k_0}}{\boldsymbol{\eta}}\frac{\partial \boldsymbol{P}}{\partial \boldsymbol{z}} \qquad \textbf{(1.4)}$$

where φ is the volume fraction of suspended particles, k_0 is the gel permeability and η is the surfactant solution background viscosity. Since the rate at which the fluid is expelled from a material element is equal to the rate at which solid enters:

$$(\mathbf{1}-\boldsymbol{\phi})\left(\frac{\partial \boldsymbol{v}}{\partial \boldsymbol{z}}\right)+\boldsymbol{\phi}\frac{\partial^{\mathbf{2}}\boldsymbol{w}^{\mathbf{2}}}{\partial \boldsymbol{z}\partial \boldsymbol{t}}=\mathbf{0} \qquad \textbf{(1.5)}$$

If $\phi \ll 1-\phi$, *Equation 1.4* implies $v \cong 0$. At short times, the gel is uncompressed and the elastic stress is negligible, so that

$$\frac{\partial \boldsymbol{P}}{\partial \boldsymbol{z}}=-\boldsymbol{\Delta\rho g\phi} \qquad \textbf{(1.6)}$$

where $\Delta\rho$ is the density difference between fluid and particles and g is the gravitational acceleration. Consequently, *Equation (1.7*) yields :

$$\boldsymbol{k_0}=-\frac{\boldsymbol{\eta}}{\boldsymbol{\Delta\rho g\phi}}\frac{\partial \boldsymbol{w}}{\partial \boldsymbol{t}}\bigg|_{\boldsymbol{t=0}} \qquad \textbf{(1.7)}$$

At long times, contributions from the network elasticity must become important, since the deformation of the network is no longer negligible. Therefore, at short times, the gravitational stress is balanced by the stress due to fluid flow, while at long times it is balanced by the network elasticity. At intermediate times we expect both to play a role. For Darcy's flow the dominant contribution to the fluid stress comes from the fluid pressure, which is much larger than the viscous stress. After some deformation, the network elasticity starts to oppose to further compression. Assuming no significant change in the particle volume fraction along the vertical axis, the overall interface changes with time as follows:

$$\boldsymbol{h(t) = h_0 + \Delta h e^{-\frac{t}{\tau}}} \qquad \textbf{(1.8)}$$

where h_0 is the e initial height and Δh is the total change in height; τ is the time scale for the collapse, calculated as follows, where G_0 is the gel elastic modulus.

$$\boldsymbol{\Delta h = \frac{\Delta \rho g \phi h_0^2}{2G_0}} \qquad \textbf{(1.9)}$$

$$\boldsymbol{t \approx \frac{4\eta h_0^2}{\pi^2 k_0 G_0}} \qquad \textbf{(1.10)}$$

Such a description is strictly valid only in the limit that the gel does not rearrange during compression. T*h*e fact that we generally observe two distinct stages in the evolution of *h*(t) is not accounted for in this model. Regardless of this obvious discrepancy between the physics underlying the model and the actually observed behavior, the Poroelastic Model is to date the only model able to describe the gravitational collapse of gels. It has been applied to describe the splitting edge, that is the variation of the temporal evolution of the height of interface of the gravitational collapse, in various stages: the initial compression (Manley *et al*., 2005), the first part of the second regime (Huh *et al*., 2007), and the final consolidation regime (Buzzaccaro *et al.,* 2012). The nature of the transition between the first and second stage is still somewhat unclear. It may be related to a cascade of yielding events on a local scale and consequent

fluidization of the fiber network, leading to global failure. Presuming that the initial stage corresponds to the time lapse during which the entire network is compressed, while in the second stage the network is broken down into clusters (that become gradually compacted), the use of the Poroelastic Model to describe both stages of the failure dynamics might be justified by assuming different porosities related to each previously described stage.

Chapter II

2. Experimental setup

For our purpose, a simplified formula of liquid detergent for washing machine is adopted; this fluid is, then, characterized in order to measure its relevant physical properties, which are used to compare the observed behavior to theoretical predictions. Since we have to study aerated products, we developed a method to obtain, from the basic model formulation, structured liquids containing different concentrations of air bubbles. We also performed experiments with solid hollow spheres, in a way to mimic the air bubbles in a controlled way and at the same time to tune the conditions at the interface and study its role on the bubble dynamics. In this way, tracking and loading tests can be performed on structured and aerated products. In this chapter all materials, experimental setups and apparatuses used in this study are described.

2.1. Materials: fluids and spherical objects

The fluid used is a simplified version of a structured Heavy Duty Liquid (liquid detergent for washing machines). The model fluid is made by a background surfactant solution, composed by an anionic surfactant, Linear Alkylbenzene Sulphonic Acid (HLAS) neutralized with Monoethanolamine (MEA) at pH = 8. Fibers are added to the solution in the form of a suspension, a premix formulation property of Procter & Gamble (Procter & Gamble, EP01396535B1, 2004) whose detailed composition is not given for confidentiality reasons. It can be said, however, that the most relevant component of the system is Hydrogenated Castor Oil (HCO), crystallized in the form of fibers. The latter have a diameter in the range of 20–100 nm and a length in the range of 1–10 μm (De Meirleir *et al*, 2014). The mesh size of the network is dependent on HCO concentration and is in the nanometer range.

The raw materials have been provided by Procter & Gamble and used as received. Samples have been prepared by gently stirring surfactant and MEA in water and adding the HCO as fast as possible and close to the impeller blade (without submerging into the liquid) in order to optimize dispersion. Samples at a fixed concentration of HLAS and MEA were loaded with various HCO weight concentrations, ranging between 0 and 4%. The density of the fluid is 1.01 g/cm^3.

To study the rising velocity of spherical bodies, hollow glass microspheres with sizes and densities reported in *Table I* have been used (Cospheric Company, Santa Barbara CA USA). A very low weight concentration of spheres has been used to avoid hydrodynamic interactions between the particles.

Diameter (µm)	**Density (g/cc)**
27-45	0.29
75-90	0.30
75-90	0.12
90-125	0.09
125-150	0.07
150-180	0.06

Table 1*: Hollow glass microspheres properties*

In several experiments, we also observe and measure the rising velocity of air bubbles that are freely entrapped in the system during the preparation stage. The air bubble diameter ranges between

200 and 550 μm, whereas the glass beads are smaller (see Table 1). In general, in experiments performed with hollow spheres, gas bubbles were avoided. When hollow spheres and bubbles were both present, the different refractive indices were used to discern between them.

It must be observed that with our systems the high surface tension of the suspending fluid and the small bubble size guarantee that bubbles can be treated as undeformable spherical objects. Indeed, following Ducloué *et al.* (2014), the Capillary number, evaluated as:

$$Ca = \frac{\sigma_\sigma R}{2\lambda} \qquad \textbf{(2.1)}$$

where λ is the interfacial tension of the suspending fluid, is in the range $10^{-7} < Ca < 10^{-4}$. Moreover, the mesh size of the network is always significantly smaller than the particle size. This guarantees that during its rising motion the particle "feels" a homogeneous network and pushes the fibers away.

2.2. Methods

2.2.1 Rheological measurements

Rheometrical tests have been performed on the fluids to determine their rheological properties and, in particular, the yield stress values. They have been performed on a stress controlled rotational instrument (MCR 702 TwinDrive, Anton Paar, Physica). Reproducibility has been checked by repeating the same test three times and by using different geometries: plate-plate (diameter 25 mm; gap 1 mm), cone-plate (diameter 25 mm, angle 0.99°) and Couette (radius of bob 13.3 mm, radius of cup 14.4 mm). Different cone angles and diameters have also confirmed the same rheological response, thus proving the absence of slip and shear-banding. Temperature has been controlled with a Peltier system and kept constant at 25°C. In order to minimize evaporation, an anti-evaporation tool has been used and a fresh sample has been reloaded for each experiment.

Measuring the viscoelastic properties of a structured system is usually difficult, since the results may depend on the preparation and the shear history of the sample, as well as on the flow geometry. The samples do not show ageing on a time scale of a year. In a way to compare all the samples at

the same initial conditions, as a protocol, all tests have been carried out after a pre-shear of 100 s^{-1} for 30 s to erase the shear history of the samples. The preshear performed on the samples does not have a fundamental role on the evaluation of the dynamic yield stress value. Indeed, the experiments performed with and without preshear are perfectly overlapping. We have performed creep tests to determine long time response and to compare the yield stress value with the one calculated through the steady experiments. We decided to use the flow curves to obtain a single yield stress value, instead of creep experiments that provide a range of yield stresses. The yield stress evaluated through the steady measurements fall within the range determined with the creep measurements. Steady-shear tests have been performed from 100 to 10^{-5} s^{-1} and the Herschel-Bulkley model has been used to fit the curves (Mullineux, 2008). The sampling time has been taken in a logarithmic scale, starting from a few seconds at the highest shear rates and increasing the waiting time for the lowest values. The reproducibility has been proven by tuning the measuring time during the flow curve and, thus, confirming the yield stress value.

2.2.2 TEM measurements

TEM measurements are executed with negative and osmium staining. The negative staining procedure consists in transferring a drop of 10 µl of sample on a perforated grid (Formvar/Carbon Membrane on 200 Mesh Copper Grids). A Glow Discharged (Mini Spec-Quorum Technologies) treatment is applied to the formvar/carbon film to make it hydrophilic before the deposition of the sample (15sec, 5 mA). After 2 minutes the excess of liquid is removed by a filter paper sheet (Whatman). Each grid is floated on a 2% uranyl acetate (Sigma, Aldrich) drop for 40 seconds, and then dried at room temperature under hood. The osmium staining procedure requires to place a 500 µl stock solution of fibers overnight in a sealed container with OsO_4 vapor (2% water solution, Electron Microscopy Sciences) in the presence of 95-97% humidity to prevent sample evaporation. A drop of 10 µl of OsO_4 stained fibers is placed on the 200 mesh Copper grid coated with formvar/carbon film after a glow discharge treatment; the excess of sample is removed by touching the edge with a filter paper sheet followed by drying at room temperature. All samples are observed using a Tecnai 20 Cryo-Tem instrument (FEI, Eindhoven) operated at 200 KV and equipped with

a LaB6 filament. Micrographs are recorded on a Gatan 2HS CCD Camera. In order to obtain quantitative information on the fiber microstructure, TEM images are analyzed by Image J (Image Processing and Analysis in Java – free download). From the heterogeneous network, it is possible to outline irregular polygons. The mesh size between the fibers is measured as the ratio between the surface and the perimeter of a significant amount of polygons for each TEM image.

2.2.3 Time-Lapse Photography Technique

A home-made time-lapse photography setup has been used to monitor the dynamics of the bubbles/spheres in the viscoplastic fluids. Mechanical stability is the most essential component in our experimental setup, which is shown in *Figure 2.1*. It consists of mechanical (Newport Corporation) and optical (Canon Brand) parts. Both camera and sample holders have been placed on a common rail. The camera holder is supported by two micrometric precision stages that allow for movements parallel to the x- and z-directions (see *Figure 2.1*). A special macro lens, specifically designed for macro-photography, has been adopted to identify microparticles (MP-E 65mm f/2.8 1-5x Macro Photo Lens). The lens provides extreme close-up imaging from a 1:1 (life-size) magnification ratio to a 5:1 ratio. The macro-lens has been mounted on a full frame camera (Canon EOS 6D), offering exceptionally high quality image. All the apparatus has been placed on a compressed air suspended optical table, in a way to minimize vibrations.

At the opposite side of the rail system, the sample stage is mounted allowing for movements along x and y directions. The sample has been placed in a polycarbonate cuvette 3.5 cm high, having a square section with sides 1 cm long and 4 optical faces. A sample holder, which can host up to four cuvettes, has been screwed onto the stage.

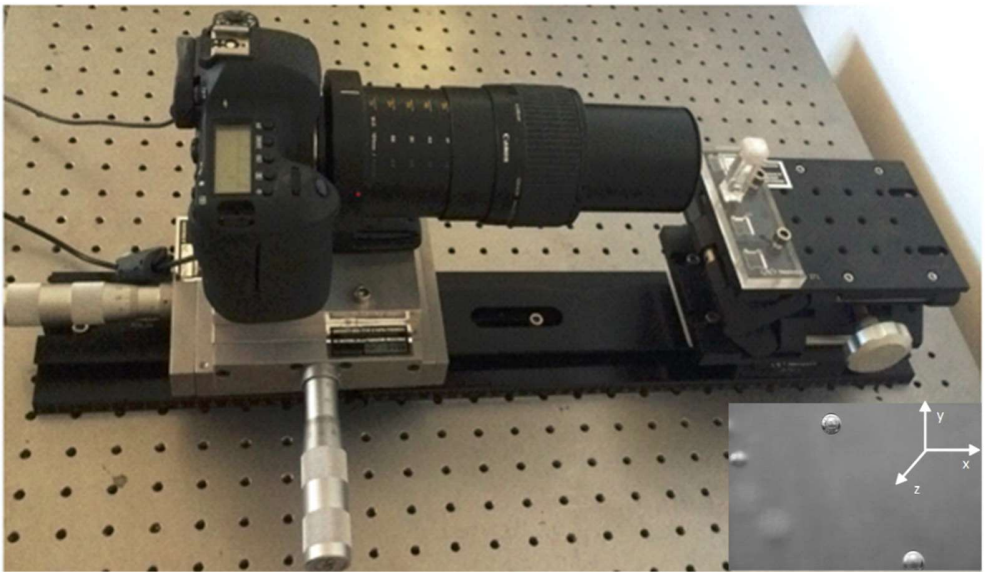

Figure 2.1*:Time-lapse setup. The directions x, y and z are depicted on the bottom-right corner. The inset is a typical image captured by the camera.*

After sample loading, the cuvette has been placed on the sample holder and single spheres have been detected by the camera. Only spheres in the middle of the cuvette have been considered in order to minimize hydrodynamic wall effects. Snapshots of the bubble/sphere motion have been taken at fixed time intervals by a specific home-made recording software.

The pictures have been analyzed by a home-made Bubble Tracking Tool, an image analysis routine able to detect a particle and to measure its position by tracking it over macro time lapse shootings. The constancy of the horizontal position over time guarantees the absence of mechanical drifts.The pixel/micrometer ratio has been measured accurately by using a micrometer optical caliper.

The software provides also a mosaic image composition of the analyzed sample. The velocity of the spheres has been calculated as the derivative of the particle trajectory as a function of time, as shown in *Figure 2.2*.

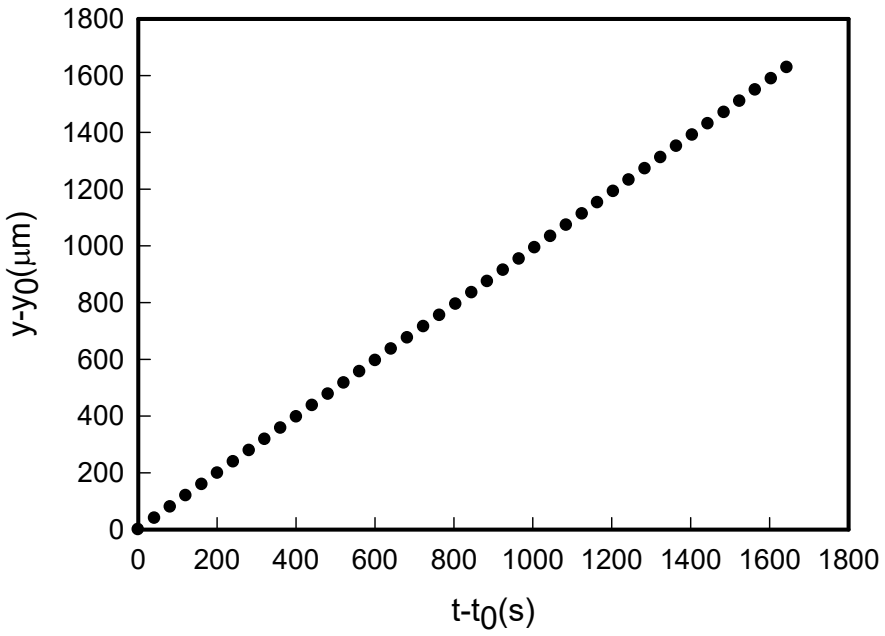

Figure 2.2**:** *Typical trajectory of a sphere over time with a diameter size of 110 μm in a fluid with a yield stress value of 0.0118 Pa.*

The apparatus has been calibrated with a model Newtonian fluid and the velocity data of spherical bodies have been successfully compared with the Stokes theoretical prediction.

2.2.4 Simulation Technique

Experimental data have been compared with finite element numerical simulations. The simulated system consists in the rising of a sphere in an infinite and quiescent Herschel-Bulkley fluid. The flow is governed by the usual conservation equations of mass and momentum for an incompressible fluid. Due to the very large viscosities characterizing the experimental fluids, creeping flow conditions are assumed. A schematic sketch of the computational domain is shown in *Figure 2.3.* A cylindrical reference frame with origin at the particle center is used. Axis-symmetry is applied along the z-direction (see *Figure 2.3*). The domain size R_d is chosen much larger than the bubble

radius R to avoid any interaction between the bubble motion and the far-field boundary conditions. Preliminary simulations show that $R_d = 60R$ is sufficient to guarantee such a condition.
Simulations have been performed by applying a force F on the particle and setting a zero-velocity field on the external boundaries far from the sphere. We consider two kinds of boundary conditions at the fluid-particle interface: no-slip (particle velocity equal to the velocity of the fluid at the solid-liquid interface – case of solid spheres) and perfect slip (no tangential stresses – case of air bubbles). For each applied force F, the corresponding particle velocity V is computed. The particle velocity V is treated as additional unknown and is included in the weak form of momentum equation. Due to the inertialess assumption, the applied force F is equal to the drag force exerted by the fluid. Such a condition is imposed through Lagrange multipliers in each node of the particle surface. More details on the numerical method can be found in D'Avino *et al.* (2010).

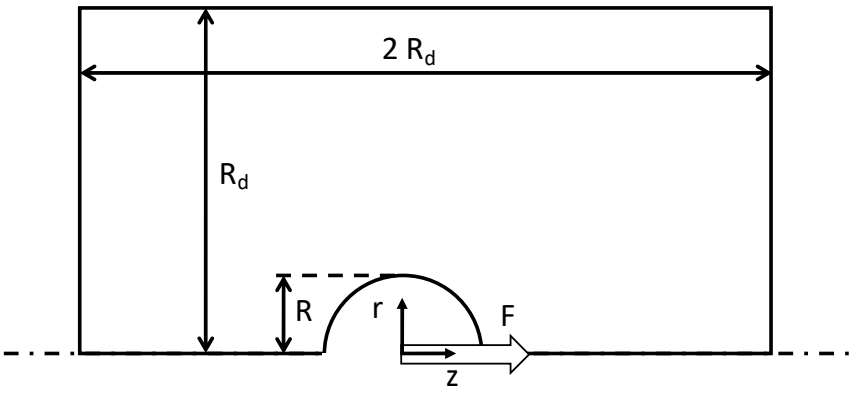

Figure 2.3: *Schematic representation of the computational domain used in the simulations. A sphere with radius R is suspended in a Herschel-Bulkley fluid. A force F is applied on the particle. The characteristic dimension of the domain is* R_d.

The fluid is described by the Herschel-Bulkley model, having the following tensorial constitutive equations:

$$\boldsymbol{\sigma} = \mathbf{2}\left(\boldsymbol{K}|\dot{\boldsymbol{\gamma}}| + \frac{\boldsymbol{\sigma_0}}{|\dot{\boldsymbol{\gamma}}|}\right)\boldsymbol{D} \qquad |\boldsymbol{\sigma}| > \boldsymbol{\sigma_0}$$

$$D = 0 \qquad |\sigma| \leq \sigma_0 \qquad \textbf{(2.2)}$$

where σ_0 is the yield stress of the fluid, K is the viscosity index, n is the power law index (Barnes, 1999), $\boldsymbol{D} = (\nabla \boldsymbol{v} + (\nabla \boldsymbol{v})^T)/2$ is the rate-of-deformation tensor with $\boldsymbol{v}$ the velocity field, $|\dot{\boldsymbol{\gamma}}| = \sqrt{2\boldsymbol{D}:\boldsymbol{D}}$ is the second invariant of $\boldsymbol{D}$, $|\boldsymbol{\sigma}| = \sqrt{2\boldsymbol{\sigma}:\boldsymbol{\sigma}}$ is the second invariant of the stress tensor $\boldsymbol{\sigma}$.

Since the Herschel-Bulkley model is discontinuous, a regularization is needed to make it numerically treatable (Mitsoulis, 2007). In this work, the Papanastasiou regularization (Papanastasiou, 1987) is adopted whereby Equations (2.2) are replaced by the following equation:

$$\sigma = 2[K|\dot{\gamma}|^{n-1} + \frac{\sigma_0}{|\dot{\gamma}|}/(1-\exp(-m|\dot{\gamma}|))]D \qquad \textbf{(2.3)}$$

where the regularization parameter m must be selected sufficiently large in order to properly approximate the original constitutive equation at low shear rates. For each imposed force F, we perform several simulations by progressively increasing the value of the parameter m until the computed velocity V does not change anymore within a certain tolerance. As expected, lower values of F require higher values of m since the regions at low shear rates have a significant effect on the drag force.

2.2.5 Aeration methods

The effect of the presence of air bubbles on the physical stability of our systems is studied by varying the aeration level. To measure it, each sample is poured in a 100 mL density cup and the aeration level is measured before and after each pouring by a specific weight static measurement. Indeed, from the specific weight of aerated samples, ρ_{Aereated}, we are able to calculate the actual total volume fraction, ϕ, occupied by air bubbles in each vials from the following *Equation (2.4)*

$$\rho_{Aereated} = \phi\rho_{AIR} + (1-\phi)\rho_{Base} \qquad \textbf{(2.4)}$$

where ρ_{air} is the specific weight of air and ρ_{base} is the specific weight of the non aerated structured samples.

Two techniques have been used to induce air bubble formation into the suspending media. One method is able to produce homogeneous bubble size; the other instead guarantees a polydisperse distribution of the bubbles into the liquid. Both methods are discussed in the following sections.

2.2.5.1 **Homogeneous bubble size**

Our aim was to compare the behavior of the hollow glass microspheres with the air bubbles in the same conditions. Bubbles with the same diameter are made with a membrane emulsification unit. The setup is shown in *Figure 2.4*. It consists of a syringe pump, a stirred cell (batch) and a microporous membrane.

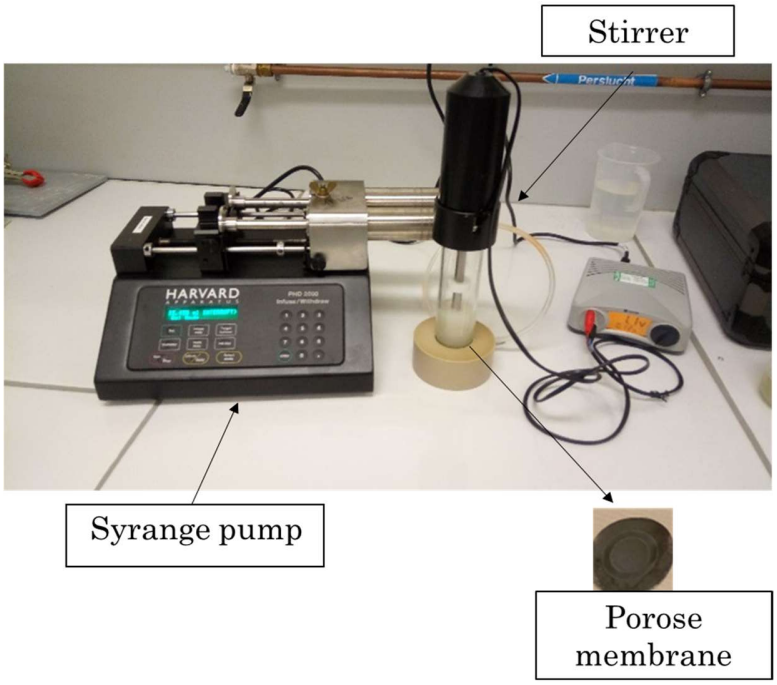

Figure 2.4: *Membrane emulsification unit setup*

The main challenge is to control the total amount of air bubbles trapped in each sample. For this purpose, various tests are performed in order to find a relation between agitation time of the stirrer and speed of the syringe pump. In our case, the air is pumped from the syringe pump at 1ml/min, and passes through the microporous membrane. The stirrer favors the detachment of the bubbles from the membrane in the continuous medium. The velocity of the stirrer is fixed at 1251 rpm. The bubble size distribution obtained from the emulsification unit is analyzed by an Image Analysis software, which is able to automatically measure the diameter of the air bubbles, which is found to fall in the relatively narrow range between 40 and 60 μm. Four fluids are analyzed containing different amounts of fibers, from 0.1 to 0.4% wt. The volume fraction of the air bubbles is fixed at 1 and 3%. The results are shown in *Figure 2.5* and the values are reported in *Table 2*. It is important to highlight that bubble dimensions have been measured at room temperature, immediately after the emulsification process.

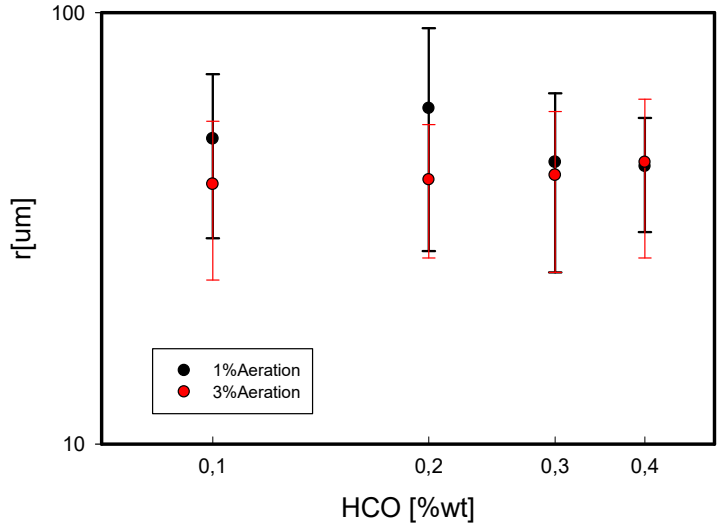

Figure 2.5:*Average radius of bubbles made by the Membrane Emulsification unit*

HCO [%wt]	1%Aeratiom- r (µm)	3%Aeratiom- r (µm)
0.1	51±21	40±16
0.2	60±32	41±14
0.3	45±20	42±17
0.4	44±13	45±18

***Table 2**: Average radius of air bubbles in different yield stress fluids*

.

The samples reported in *Table 2* are used to perform loading tests at different room temperatures (T= 25-30-50°C) with a time lapse apparatus. In our setup, a Reflex Camera (Canon EOS 600D), remote controlled, is able to capture images at regular user-set intervals. In our case the pictures are taken each day for a time period of roughly 4 months. The tests are performed with a fixed vial long 6.5 cm and a circular section. In addition to this, each vial is sampled before loading tests in order to provide the bubble size distribution of each tested fluids and to recognize the features of bubbles fractions trapped into the fluid, due to the yield stress presence.

2.2.5.2 **Heterogeneous bubble size**

Aerated samples with a polydisperse bubble size distribution were simply obtained by high rpm stirring during the making process of the sample, immediately after the addition of the HCO fibers to the surfactant solution. Obvioulsy, in this case it is not possible to control the bubble size distribution.

Forty five different samples, with fiber content from 0.2 to 0.4% wt and air bubble volume fractions ranging from 2% to 5%, are used to study the effect of air bubbles on their physical stability at different temperatures (T=25-30-50 °C). The tests are carried out for more than three months.

Chapter III

3. Rheology of fiber suspensions based on micellar solutions with different surfactant content

In this chapter, various systems are studied by tuning LAS and HCO concentrations to evaluate the contribution of surfactant and fibers on the resulting rheological response. The rheological properties of these systems are evaluated using a combination of oscillatory and steady shear flow measurements. Information on the fiber network has been obtained by electron microscopy images (TEM).

3.1. Microscopy data

TEM images of selected samples at fixed LAS concentration and different HCO concentrations are shown in *Figure 3.1.* The rod colloids are represented in white whereas the surfactant solution and residual dye are in black. The fibers are micrometer long whereas their diameter is in the nanometer range, as already proven elsewhere (De Merleier *et al.,* 2014). As the concentration of the fibers increases, the network becomes tighter and tighter and fibers start to bundle creating an interconnected "sponge" with many branches. At concentration of [HCO] = 0.3%, *Figure 3.1(a)* shows a network with a well-defined mesh size. At the maximum concentration (*Figure 3.1(b)*), fibers create tighter tangles. A network-like system can still be identified characterized by a smaller mesh size.

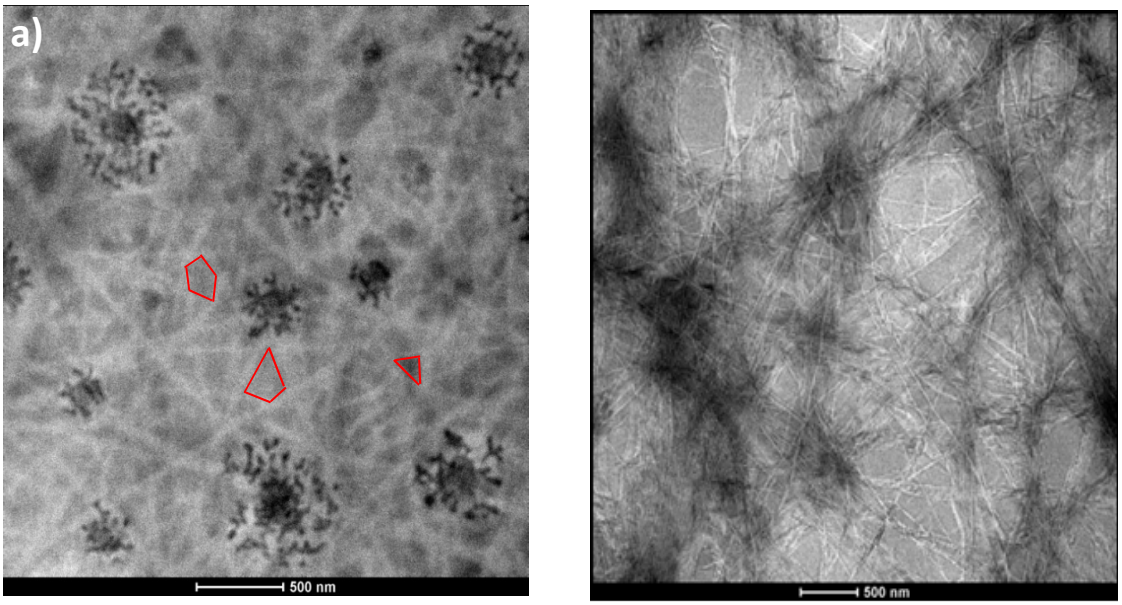

Figure 3.1: *TEM images of the solution of a) 0.3%HCO b) 4%HCO. The red lines are examples of irregular polygons tracked to measure the mesh size between the fibers.*

To quantify the mesh size *l*, we have analyzed TEM images with the Image J software (see details in the Material and Methods section). We have fitted the distribution of the fiber network at each concentration obtaining l=42±5 nm for [HCO] = 0.3% and l=6±2 nm for [HCO] = 4%. The mesh size decreases with increasing fiber concentration, with a power law index of -0.75, although obtained only for two points, proving that the network system is becoming tighter.

3.2. Rheology data

In this work, surfactant and fiber contributions are studied in order to characterize the mechanical proprieties of the system. We explored the phase behavior of LAS and HCO/LAS systems over a wide range of parameters. The dependence of the viscosity on LAS-concentration exhibits the typical features expected for micellar systems that gradually evolve from spherical micelles to

worm-like micelles and, eventually, to branched ones as the concentration further increases (Dreiss, 2017).

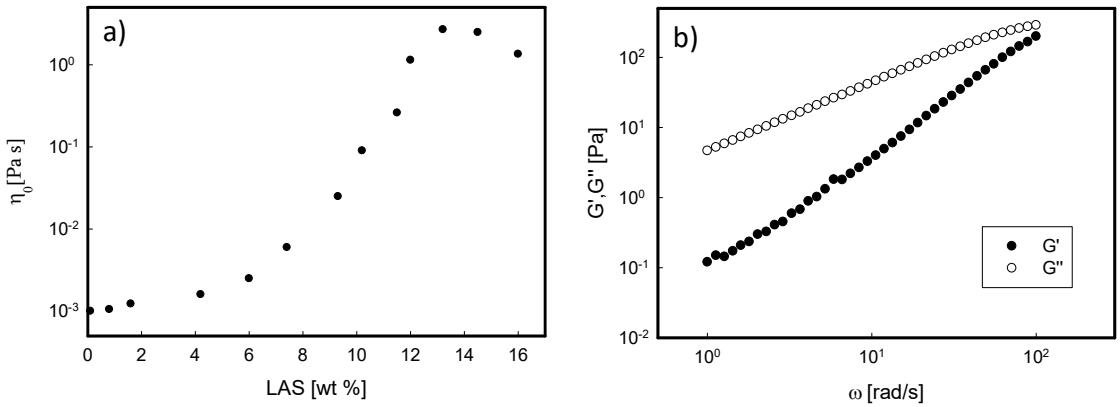

Figure 3.2: *a) LAS-concentration dependence of zero-shear viscosity of LAS solutions at T = 20°C. b) Linear mechanical response of the sample at 13% [LAS], strain 0.5%.*

As shown in *Figure 3.2(a),* the zero shear viscosity only slowly increases with concentration in the range of [LAS] < 5% to then increase by more than 3 orders of magnitude in the concentration range of 5-13%. This transition from moderately increasing to strongly increasing viscosity is generally assigned to the formation of worm-like micelles that increase in length as the concentration is increased, thereby becoming strongly entangled. In the latter case, their relaxation is determined by both breakage and reptation of the micelles along their own contour-length (Dreiss, 2007); Cates *et al.*, 1990). In the wormlike micellar phase, the rheological response can be considered as Maxwellian. An example of a typical rheological response is shown in *Figure 3.2(b)* for [LAS] = 13%. At LAS concentrations exceeding 13% we find that the viscosity slightly decreases, a behavior that can be assigned to the abrupt decrease in contour length (Dreiss, 2007) or to the formation of branched micelles, characterized by an extra relaxation mode given by the sliding of the branches along the main backbone. *Figure 3.3* shows the relaxation time and the high frequency elastic plateau modulus as function of the LAS concentration, obtained via frequency sweep data. The relaxation time follows the same trend of the viscosity whereas the

elastic plateau increases with increasing LAS concentration, reaching a plateau value as LAS exceeds 14%. This justifies the morphological transitions already explained before.

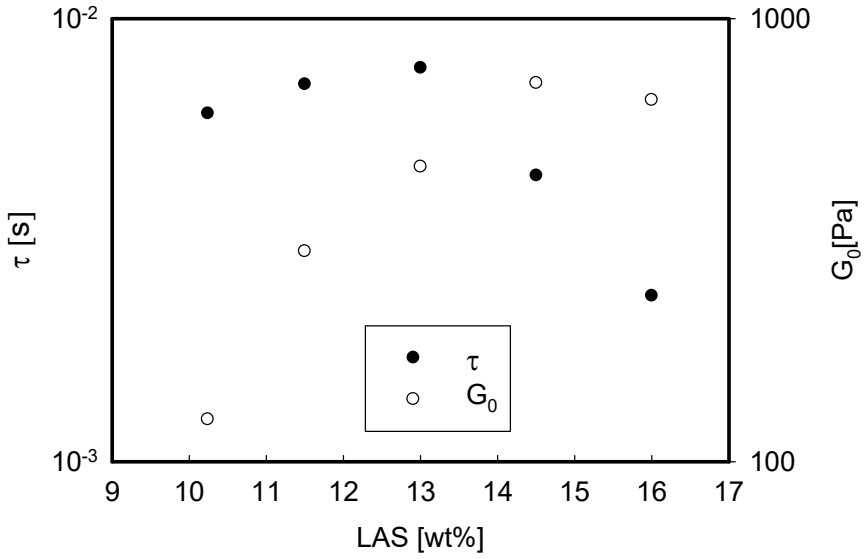

Figure 3.3: *LAS-concentration dependence of relaxation time (left axis) and elastic plateau modulus (right axis) at T = 20°C.*

At concentrations larger than 16% (not shown in *Figure 3.3*) LAS forms lamellar phases and solutions become turbid. The solution with LAS at 16% has been considered as the base solution to study the effect of the HCO fibers content on the rheological response. In *Figure 3.4*(a) the steady-state viscosity at different fiber concentrations is reported to demonstrate the structuring effect of the fiber network. The base solution (no fibers, 16% LAS) displays a Newtonian behavior. Upon increasing the fiber concentration, the material shows a strong shear thinning. When data are plotted as shear stress vs. shear rate (see *Figure 3.4(b*)), the HCO concentration dependent yield stress value is clearly detected. As shown in *Figure 3.4(b)* the yield stress value strongly increases upon increasing the HCO content. As explained elsewhere (Mirzaagha *et al.*, 2017), the yield stress value can be extrapolated by fitting the data with a Herschel-Bulkley model (see Materials and Methods section).

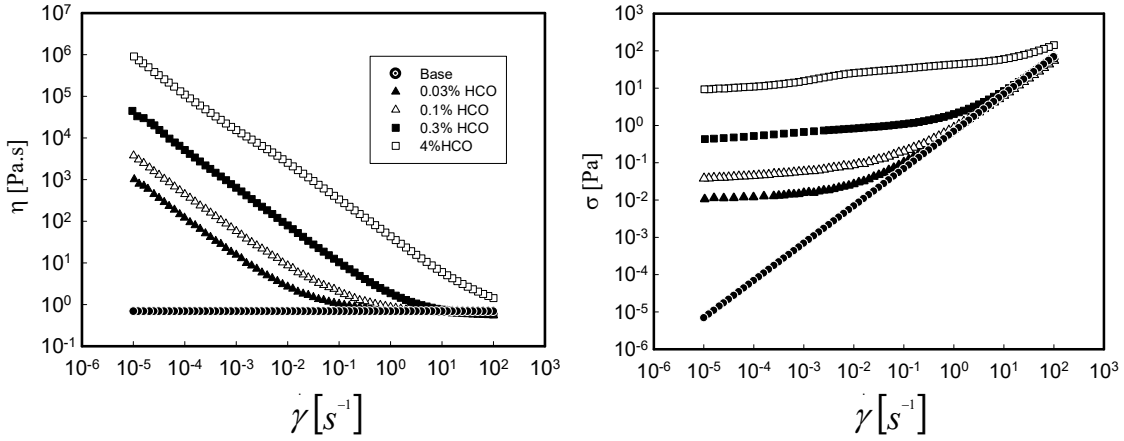

Figure 3.4:*Flow curves at different concentrations of HCO [0-4%] 16% LAS (see legend for details): a) viscosity versus shear rate b) shear stress versus shear rate. The dash-dot line is Herschel-Bulkley fit.*

In order to understand the rheological influence of the fibers over the surfactant background, a comparison between the oscillatory response of structured and unstructured samples is carried out, as reported in *Figure 3.5*.

In *Figure 3.5(a)*, at low frequencies the suspensions are clearly elastic: the storage modulus (G') has no frequency dependence, leading to a plateau modulus G_0. As expected, the plateau storage modulus increases with fiber concentration. *Figure 3.5(b)* shows the loss modulus of the solutions. At high frequencies the loss moduli of the samples seem to approach a limiting, concentration independent value, whereas at low frequencies the effect of network formation, already seen in the elastic modulus, again appears, although to a minor extent.

It can be generally concluded that in our structured samples at low frequency the elasticity of the network dominates, while at high frequency the viscoelasticity of the worm-like micellar background prevails.

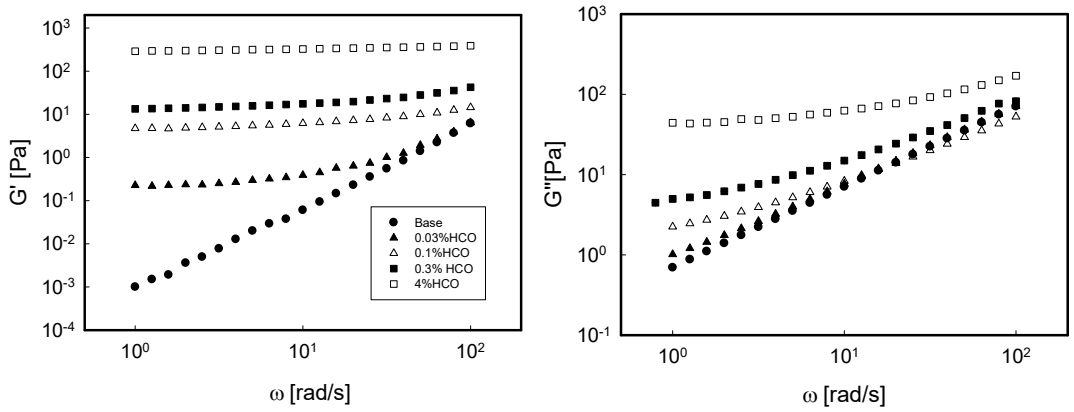

Figure 3.5:*Rheological behavior at different HCO [0-4%] (see legend for details): a) Storage G' and b) Loss moduli G'' as function of frequency***.**

In order to better understand the influence of the fibers on the rheological properties of the surfactant suspending medium, a comparison between the plateau modulus $G_{0,}$ calculated from the oscillatory response, and the yield stress value σ_0 taken from the steady shear rate experiments is reported in *Figure* 3.6 as a function of HCO concentration.

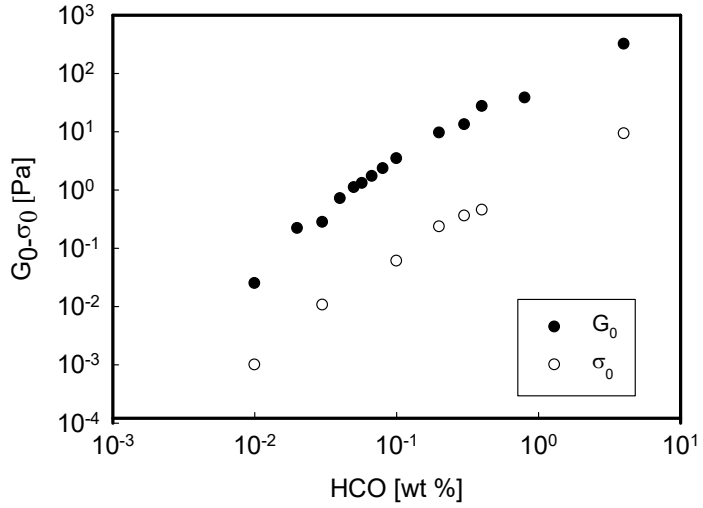

Figure 3.6: *Comparison of elastic modulus and yield stress value at different HCO composition.*

The trend with HCO content is the same considering both rheological parameters, with G' always exceeding the yield stress value. The data set are lying on straight lines in a double logarithmic scale, characterized by the same slope, except for the points corresponding to the lowest concentrations. This could suggest the presence of a critical concentration for the onset of elasticity, which could depend on the surfactant content. As such, we decided to perform the same test for different LAS content and various HCO concentrations. *Figure* 3.7 (a) shows the low frequency elastic modulus G_0 obtained in oscillatory strain experiments performed in the linear regime as function of the HCO content and parametric in the LAS concentration. The elasticity of the HCO network exhibits a critical onset and growth at a critical HCO value that depends on the surfactant concentration. LAS does not only determine the viscosity of the system, but also indirectly contributes to elasticity. For a given LAS-concentration we typically observe that the system requires a minimum amount of HCO to exhibit elastic properties. Beyond this critical concentration, indicated in the following with $[HCO]_c$, the elastic properties first strongly increase with [HCO] to then increase slightly faster than linearly at larger concentrations. The critical onset and growth of the elasticity is a function of [LAS]; the larger [LAS], the smaller $[HCO]_c$.

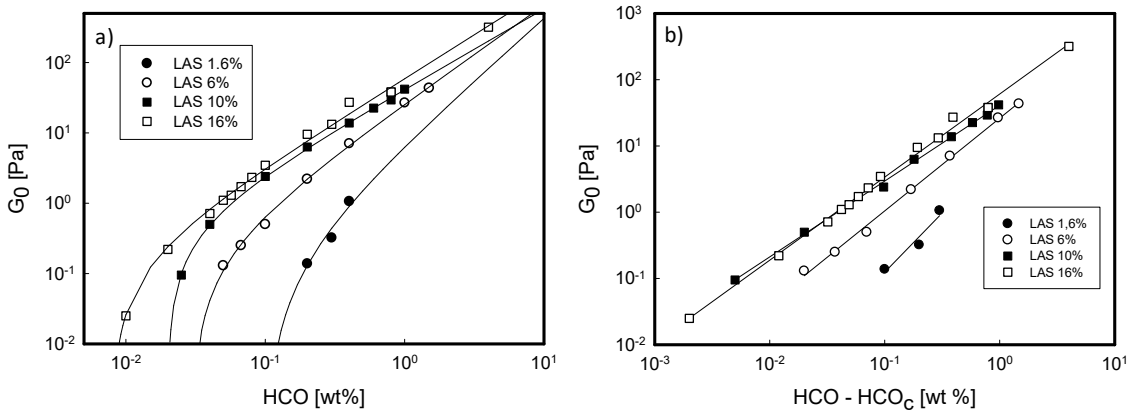

Figure 3.7: *a) Low frequency modulus of fiber network G_0 as a function of HCO-concentration for HCO/LAS-systems with LAS concentrations as indicated in the legend. The solid lines are fits to the data according to $G0=A([HCO-HCO])^{\alpha}$ b) Same data as in (a) reported as a function of the reduced concentration $[HCO]-[HCO]_c$ to demonstrate the validity of using a critical-like function to describe the [HCO]-dependence of G_0. Black lines are linear regressions.*

It is possible to scale out the dependence on HCO concentration by subtracting $[HCO]_c$ for each data set. The result is shown in *Figure 3.7(b)* for the various LAS concentrations, where the plateau modulus is plotted as function of $[HCO]-[HCO]_c$. The behavior can be modeled with a power law dependence of the plateau modulus on the [HCO] content, $G_0 \sim C^{\alpha}$, and the fits are reported along with the data in *Figure 3.7(b)*. The exponents obtained are of order of α = 1.1-1.8. Although the slope seems to be dependent on LAS concentration, *Figure 3.7(b)* shows that at LAS concentration higher than 10%, the dependence on the surfactant content is negligible. In this concentration range, G_0 data are compared to the data by Merleier *et al.* (see *Figure 3.8*), who studied the rheological behavior of surfactant – water solutions containing different crystal shapes of HCO. They performed frequency sweep tests for each suspension composition and for HCO concentrations ranging from 0.08 to 3%, by keeping fixed [LAS] =12%. The elastic modulus does not reach a constant zero slope at low frequency ($G_0 \sim \omega^n$, ω is the angular frequency and $0.17<n<0.22$). As such, Merleier *et al.* evaluated G_0 at a fixed angular frequency of 0.628 rad/s. Using these data, they found that α depends on the HCO content and is 1.52 for fiber content between 0.01% and 0.1% and 0.94 for HCO concentration between 0.1% and 3%. Therefore, they experimentally found a double slope for G_0 *vs* HCO content. A direct comparison between their data (performed at [LAS] = 12%) and the experimental measurements of the present work at two different LAS concentrations, 10% and 16%, is shown in *Figure 3.8.*

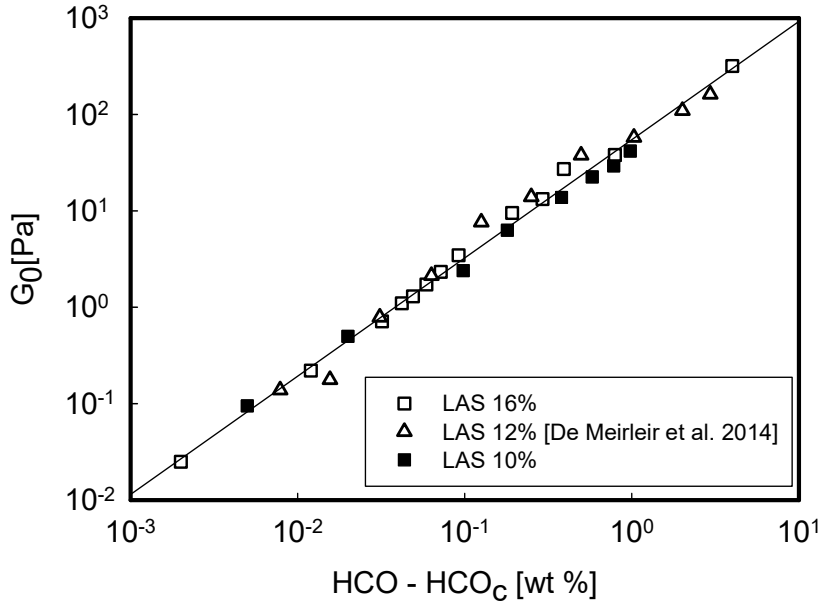

Figure 3.8:*Elastic modulus as function of HCO composition. Circles are current experiments at [LAS] =10% and [LAS] =16% (see legend for details). Hollow Triangles: experimental data from De Meirleir et al.(2014). Black line is the linear regression fitting*

On the one hand, the quantitative overlap between our data and data by Merleier *et al.* is apparent. On the other hand, in our systems, the difference in slope according to the HCO range concentrations is not at all apparent. Looking at our wide range of data, it seems from *Figure 3.8* that the power law is characterized by a unique power index for the whole [HCO] range, equal to 1.23. Nevertheless, the value of α from the fit of our experimental data at [LAS] =10% and 16% is close to the value calculated by Merleir *et al.* at [LAS] = 12%, in the low concentration regime (1.23 *vs* 1.52). Therefore, we tend to conclude that the concentration dependent slope determined by Merleier *et al.* is possibly due to the way the elastic plateau has been evaluated or it is an artifact caused by the inevitable scattering of the experimental data points.

The systematic shift of $[HCO]_c$ with increasing [LAS], shown in *Figure 3.8*, demonstrates that LAS induces attractive interactions among the fibrillar clusters. It is reasonable to assume that these attractions are due to depletion phenomena. Depletion interactions are generally induced when larger colloidal entities coexist with smaller entities. In such a case, there is a net gain in free volume for the smaller species when the colloids cluster together, which effectively results

in net attractive interaction between the colloids (Poon, 2002). In the HCO/LAS-systems, LAS acts as a depletant and we can estimate the strength of interactions as $U_{depl} = \Pi V_{overlap}$ with Π the osmotic pressure of the LAS-micelles in the background medium and $V_{overlap}$ the overlap volume defining the volume around the HCO-fibers, from which the center of mass of the micelles is excluded. In the semidilute regime of worm-like micelles we can assume that $\Pi \sim \xi^{-3}$, with ξ the correlation length exhibiting a scaling behavior with surfactant concentration "*s*" that depends on the flexibility of the micelles, $\xi \sim s^{-0.5\text{-}1}$ (Berret, 2006). For the overlap volume of the fibrillar HCO, we assume $V_{overlap} \sim \xi$, such that $U_{depl} \sim \xi^{-2}$. To account for the impact of this interaction on the elastic properties of the network, we can consider that the absolute magnitude of the modulus is set by the spring constant k_0 defining the resistance to bond-stretching. Taking into account that the range of the depletion interaction is set by ξ, the spring constant can be estimated as $k_0 = U_{depl}/\xi^2 \sim \xi^{-4}$, such that we expect $G_0 \sim \xi^{-4} C^{\alpha}$, where "C" is the HCO concentration The elastic modulus has been found to scale with the surfactant concentration as $G_0 \sim s^{9/4} C^{\alpha}$. Such scaling relation describes the dependence on *s* remarkably well: a normalization of G_0 with $[LAS]^{9/4}$ leads to an almost perfect collapse of all data sets obtained at different [LAS], as shown in *Figure 3.9*. This would indicate that $\xi \sim s^{-9/16}$.

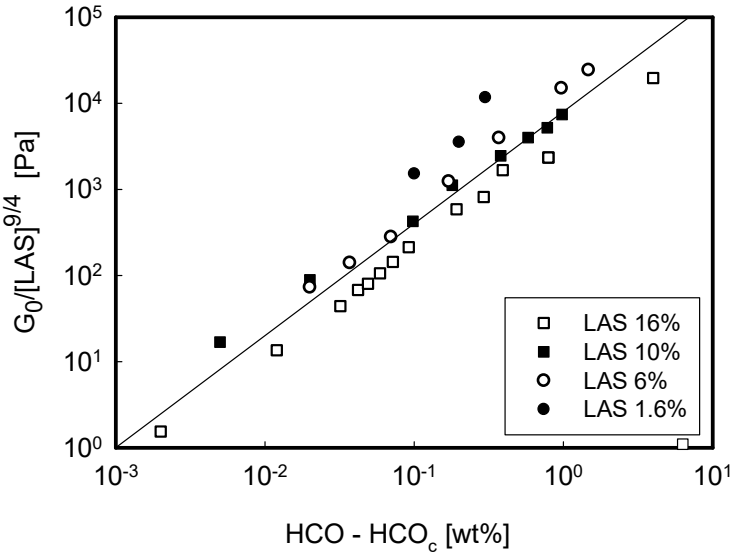

Figure 3.9: *Same data as in Figure 3.5 where the elastic modulus is normalized by $[LAS]^{9/4}$. For the normalization we use [LAS] in weight fraction rather than weight percent generally used in this report. The solid line corresponds to $G0/[LAS]^{9/4} = 4900\ [HCO]^{1.58}$.*

Chapter IV

4. The rising motion of a single sphere in structured fluids with yield stress

Various yield stress values will be analyzed and, through a home-made time-lapse apparatus, the rising velocity of spherical bodies of different sizes will be measured. The experimental data are compared with numerical predictions from finite element simulations, assuming both interfacial slip and no slip conditions. To highlight the contribution of the power law index "n" for a Herschel-Bulkley fluid, the results of the present work are compared with the experimental data and theoretical predictions coming from Tabuteau *et al.* (2006). Experimental and numerical results are interpreted and discussed in terms of correlations, involving the relevant dimensionless parameters.

4.1. Experimental rising velocities of spherical bodies

Optical experiments are performed by analyzing spherical particles in the above-mentioned fluids. In each sample, we observed both the motion of air bubbles and of hollow glass microspheres. The pictures are taken over different time periods, from several hours to several weeks and the particle trajectory is reconstructed. After a very short transient time, the spherical bodies either reach a steady, terminal rising velocity or they remain still in the fluid.

Figure 4.1 shows the experimental terminal velocity of the rising spherical objects as a function of the particles size, for different values of the fluid yield stress. The rising velocity changes by four orders of magnitude. The smallest velocity is of the order of 10^{-3} μm/s. This actually translates in an experimental time of roughly 50 days. All the spherical objects that do not move in this time frame are considered immobile.

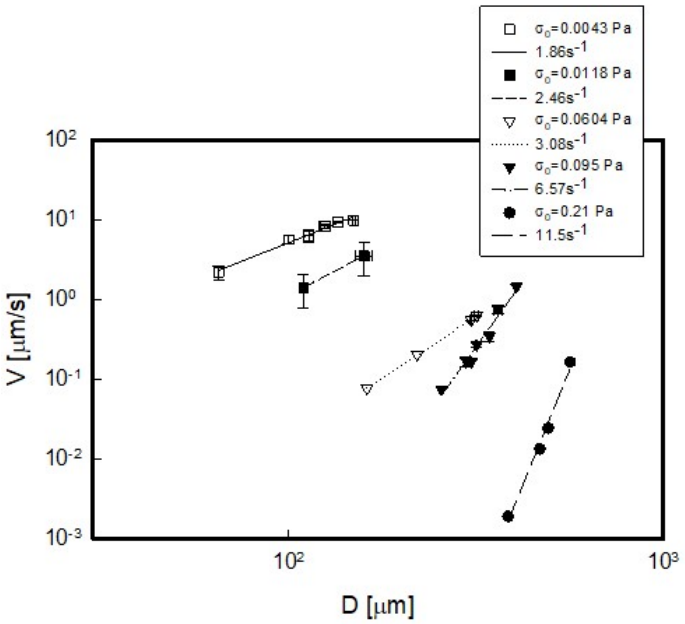

***Figure 4.1**: Terminal velocities of spherical particles and air bubbles as function of the particle diameter for different fluids (corresponding to different values of the yield stress). Lines are linear regression through the data. The legend shows the slope of each relative data set.*

Figure 4.1 clearly shows that both spheres size and yield stress value play a significant role in determining the rising velocity. As expected, a higher yield stress and a smaller sphere diameter lead to lower terminal velocities.

It is worthwhile to point out that, although the experiments have been performed with all possible combinations of particles and fluids, only the hollow glass spheres with a particle diameter larger than 65 μm (see *Table 1*) effectively rise due to buoyancy, at least in our experimental time window. Moreover, the displayed data referring to a diameter larger than 200 μm are only air bubbles.

The slope of each curve has units of a rate and the linear regression provides a characteristic shear rate for the specific yield stress fluid. This shear rate increases with increasing yield stress value and the results of a linear regression for each data sets are shown in *Figure 4.1*.

4.2. A dimensionless approach

The experimental results shown in *Figure 4.1* confirm many of the observations reported in the literature for homogeneous yield-stress fluids:

- the bubbles move only when they are large enough (at least in the time frame explored in this work);
- the critical sphere diameter for motion, which is the first data point in each data set, strongly depends on the fluid properties, in particular on the fluid yield stress;
- when the particle is able to move, the velocity depends also on the size of the spherical object;
- the characteristic shear rate coming from the fit for each fluid can be compared with the corresponding flow curve (*Figure 3.4*): the shear rate value "falls" in the range of shear rates between the yield stress plateau (no flow) and the linear regime (flow). Therefore, it can be considered as a threshold value, below which the particle is not able to move in the specific suspending medium.

These experimental data are now compared with simulation results obtained by assuming that the suspending fluid is well described by the Herschel-Bulkley constitutive equation. Following previous works (e.g., Beris *et al*., 1985; Beaulne and Mitsoluis, 1997; Tabuteau *et al.*, 2006), we plot the data in terms of three dimensionless numbers for a Herschel-Bulkley fluid:

- the Stokes drag coefficient:

$$C_s = \frac{F}{6\pi K V^n 2^{1-n} R^{2-n}} \qquad \textbf{(4.1)}$$

- the Bingham number:

$$Bi = \frac{\sigma_0}{k\left(\frac{V}{D}\right)^n} \qquad \textbf{(4.2)}$$

- and the yield stress ratio, already proposed in *Equation (1.2)*

Notice that the definition of C_s is the same used by Beaulne and Mitsoluis (1997) with the drag correction factor (denoted by *X(n)* in their paper) set to one. This coefficient is an empirical parameter dependent on the power law index *n* (Dezhi and Tanner, 1985). For our fluids, such a coefficient is between 1 and 1.2 and, as such, its variation can be neglected. The Bingham number in *Equation (4.2)* compares the yield stress of the suspending fluid to the shear stress determined by the relative motion between fluid and sphere.

The same data shown in *Figure 4.1* are plotted in dimensionless form in *Figure 4.2* in terms of Stokes drag coefficient as a function of the yield stress ratio. In the same figure, the results of the finite element simulations are plotted as lines.

The simulation curves refer to two values of the power-law index (n = 1 and n = 0.8) and to both no-slip and perfect slip boundary conditions on the spherical surface. First of all, we remark that the black curve (no-slip condition and n = 1) quantitatively agrees with previous simulations (Beaulne and Mitsoulis, 1987), validating the code.

The following observations can be made:

- The whole experimental data set shown in *Figure 4.2* all collapse on a single curve if plotted in a dimensionless fashion. Moreover, the data are well described by the simulation data in the case of no slip conditions.
- The agreement between simulations and experimental data suggests the goodness of the rheological yield stress evaluation.
- From a simulative point of view, solid spheres and air bubbles behave differently. The different $Y_{c,cr}$ value for bubbles and spheres, as shown by the vertical asymptote in *Figure 4.2* (and already discussed in the introduction), confirms the theoretical and experimental results obtained in the literature (Beris *et al.*, (1985); Tsamopoulos *et al.*, (2008); Sikorski *et al.*, (2009)).
- At a fixed yield ratio, the bubbles move faster than the spheres. This is expected as the drag force on a sphere in a Newtonian liquid is 2/3 of the Stokes drag where perfect slip holds

at the particle-fluid interface (Luo and Pozrikidis, 2008) (see the horizontal asymptote for $Y_c \rightarrow 0$).

- The power law index does not have a significant role on the rising spherical body motion, at least in the range evaluated.

In *Figure 4.3* the experimental data are shown in a different fashion, where the yield ratio is plotted as function of the Bingham number. The line passing through the data is representative of the simulations, previously discussed, in the case of no-slip condition and n=1. Along with the results of the present work, experimental data and theoretical predictions coming from Tabuteau *et al.* (2006) are plotted. They are, at the best of our knowledge, the most extensive data in literature, based on a Carbopol gel solution characterized by a power law index equal to 0.5. The theoretical prediction is based on the findings of Ansley and Smith (1967):

$$\frac{1}{Y} = 6kX(n) + \frac{6X(n)}{Bi} = 7 + \frac{8.52}{Bi} \qquad \textbf{(4.1)}$$

where the drag correction factor *X(n)* is 1.42 for *n*=0.5 (Dezhi and Tanner (1985)). Simulations have also been performed with *n*=0.5 and they are shown with a dashed line in *Figure 4.3*. It is possible to draw the following conclusions:

- there is a good quantitative agreement between the experimental data and the numerical results in the case of no-slip conditions, despite our data are also on gas bubbles. A possible explanation of this phenomenon can be given by the surfactant molecules present in the solution, which could move towards the air/fluid interface and actually stiffen it (Denkov *et al*. 2009). In addition, we deal with small air bubbles, moving slowly, that can be treated as undeformable spherical objects and for which the condition of no-slip may work. These are just speculations and the absence of experimental data in literature on small not deformable gas bubbles makes the issue slip/no-slip condition even more complicated to be resolved.

- Comparing our experimental data with the data coming from Tabuteau *et al.* (2006), it is clear that our results widen the operative Bingham number window by several orders of magnitudes.
- At high and low values of Bi the effect of the power law index is negligible, as shown by the overlap between the theoretical prediction by Tabuteau el al (2006) and our work. Indeed, at Bi approaching zero, the fluid behaves as purely viscous, whereas at high Bi the viscous component in the Herschel-Bulkley model is completely suppressed by the fluid yield stress. At intermediate Bi, the power law index becomes relevant and this is apparent by the mismatch between Tabuteau *et al.* (2006) and our data. The simulations performed at n=0.5 in the intermediate Bi fall slighlty below Tabuteau *et al.* (2006) data, confirming the dependence on n. Finally, at low Bi numbers, the data of Tabuteau *et al.* (2006), based on metal spheres of centimeter size, deviate from simulations probably due to the increasing importance of inertial effects as the velocity increases.

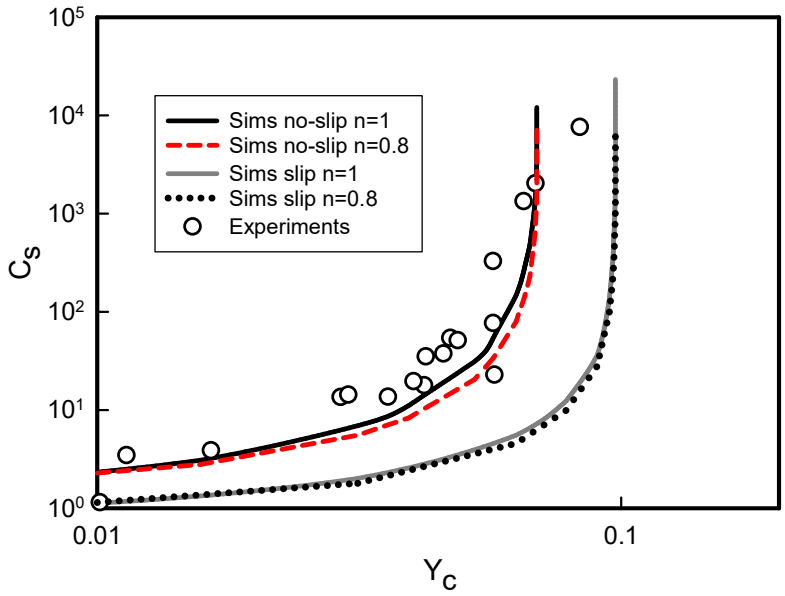

Figure 4.2: *Stokes drag coefficient as function of the yield ratio. Empty symbols: experiments. Lines: simulations with different fluid-particle boundary conditions and power-law indices n.*

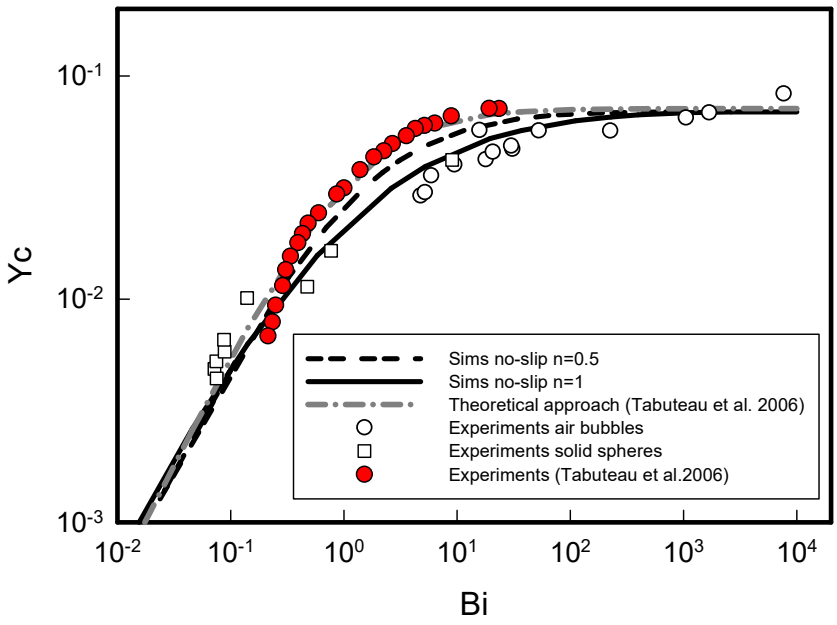

Figure 4.3: *Yield stress ratio as function of the Bingham number. Empty symbols: current experiments. Squares: hollow spheres. Circles: air bubbles. Red symbols: experimental data from Tabuteau et al. (2006). Solid line and long dashed back line: simulations with no-slip boundary conditions and power-law index n=1 and n=0.5, respectively. Dashed dotted grey line: theoretical approach following Tabuteau et al. (2006), with n=0.5.*

Chapter V

5. Stability under collective spherical bodies load

The cooperative effect of the particle ensembles have been analyzed by the home-made time lapse photography technique, previously presented, in a way to study the dynamics of the spherical bodies and to verify the possibility of a microstructure collapse in the presence of a consistent number of spheres. The experiments last as long as several weeks. The edge split during phase separation has been monitored by changing various parameters such as temperature, aeration content and fluid yield stress. The results are novel for the peculiarity of the system and for the wide range of aspects used to study the phenomenon. The results will be presented in the following sections by treating solid bodies and air bubbles, separately.

5.1. Stability under hollow glass microspheres

The initial rate of compression of the gel is determined by three parameters: the applied load; the background viscosity and the structure of the network. In this paragraph, we address the problem of our fluid collapse by presenting a series of experimental observations. The load applied to the HCO-system has been introduced by including hollow glass microspheres into the preparation, the load being controlled by the amount of spheres included *vs* the HCO content. This is similar to the classical experiments that probe the collapse of colloidal gels under their own weight; here load and structure are coupled, as they are both set by the particle volume fraction.

We use three different sets of hollow glass microspheres (see Materials and Methods Chapter), with different diameter and density values.

- Diameter 27-45 μm, density 0.292 g/cm^3

- Diameter 75-90 μm, density 0.12 g/cm^3
- Diameter 90-125 μm, density 0.09 g/cm^3

These experiments were performed in a cuvette with a square section of 1cm^2, a height of 3,50 cm and 4 optical faces. The time lapse set up (see Material and Methods) was placed in an oven at 40°C. Twelve structured samples have been studied for about 30 days, changing the size and the volume fraction of the entrapped particles. According to the motion model of the single bubble described above, we used a particle diameter such that the single sphere would not rise in the fluid. Tests are carried out with samples at [HCO] = 0.2% and 0.4% and fixed surfactant concentration [HLAS] = 16%. The the yield stress values at 40 °C are 0.14 Pa and 0.27 Pa, respectively. In *Figure 5.1* some examples of the splitting edge evolution as function of the time are reported and the properties of the samples are shown in *Table 3.*

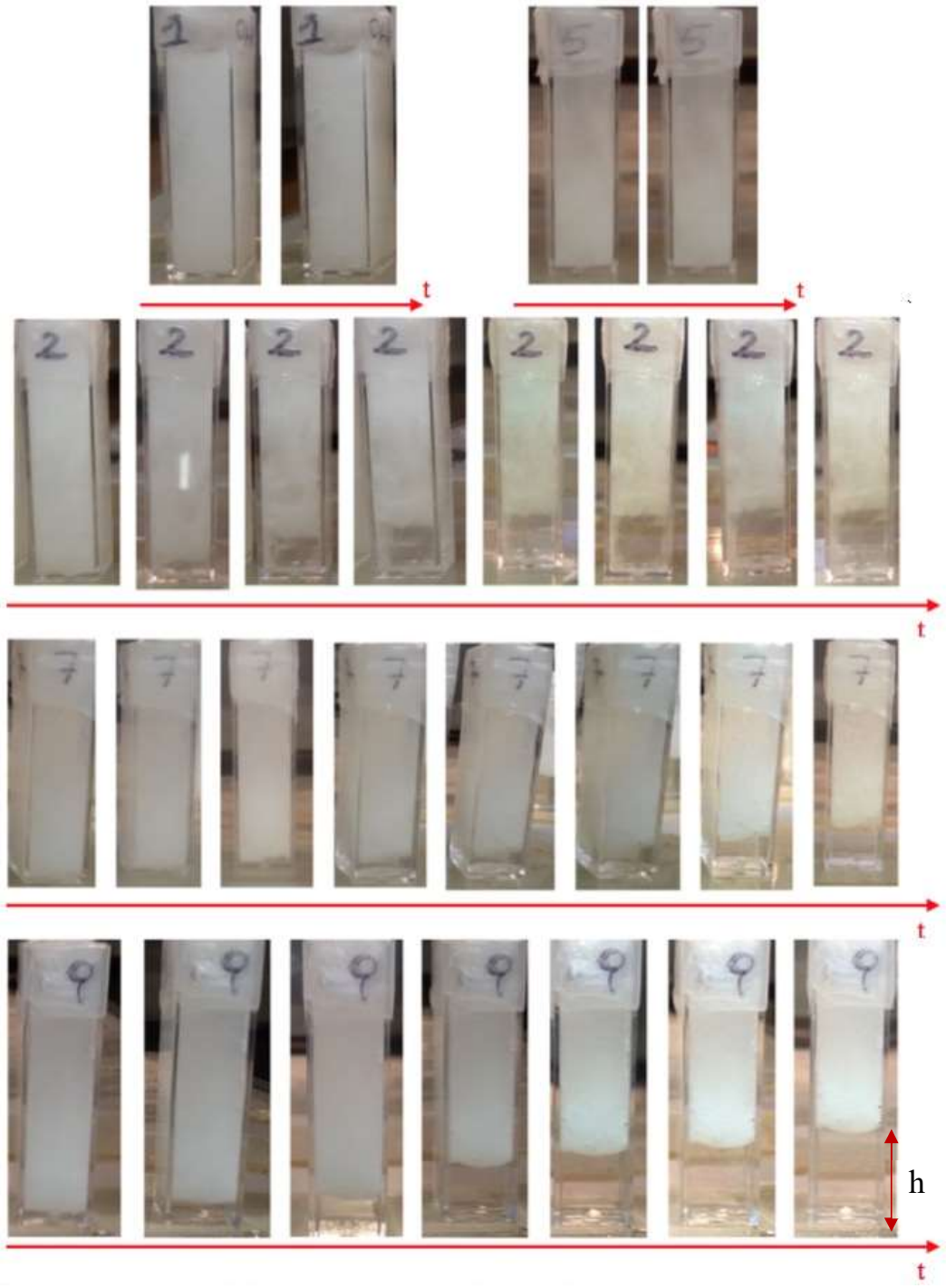

Figure 5.1: *Loading tests at 40°C. Samples 1 and 5 are stable. Samples 2, 7, 9 show a gravitational collapse. "h" shows the splitting edge of the gravitational collapse.*

Number	Sample	Volume fraction(ϕ)	Diameter (d)
1	0.4% HCO	2.5%	27-45 μm
5	0.2% HCO	1%	27-45 μm
2	0.2% HCO	4%	27-45 μm
7	0.4% HCO	2.5%	75-90 μm
9	0.2% HCO	4%	75-90 μm

***Table 3**: Samples properties for the systems analyzed in Figure 5.1*

All test results at 40 °C are shown in *Figure 5.2*, in a sort of "phase" diagram where different instabilities are indicated with different colors. The sharp phase separation with a defined moving boundary (i.e. a network collapse) is shown in red color, whereas the presence of regions of different density, typical of flocculation, is represented in yellow. The stability phenomenon is shown by a green symbol.

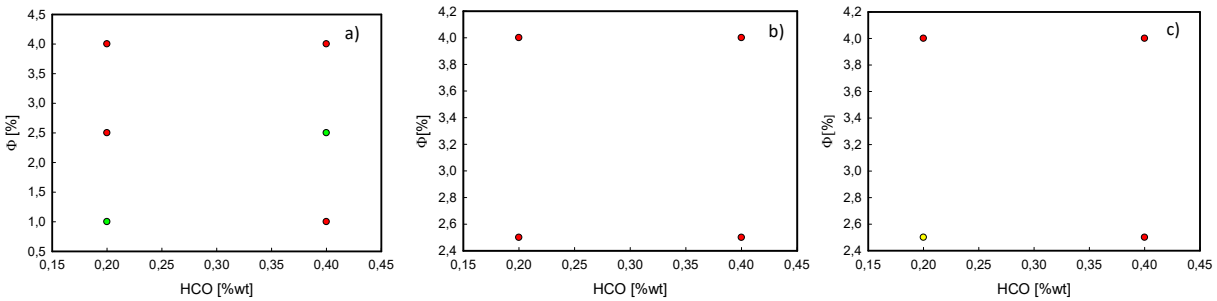

***Figure 5.2**: Stability Phase diagram: yellow or red dot means that a failure occurs in the related samples (flocculation and collapse, respectively) whereas a green symbol indicates that the relative samples are stable. The sphere size is fixed for each diagram (a) 27-45μm b) 75-90 μm c)90-125 μm*

Only two tests show a physical stability in 30 days, while all the others are unstable.

The splitting edge of the gravitational collapse has been measured as function of time and the instability is determined by two parameters: the applied load (volume fraction and spheres size) and the fluid rheology (yield stress). In *Figure 5.3*, the sphere properties are fixed, whereas the

yield stress of the fluids and the volume fraction of the spheres have been changed. From the slope of the splitting edge as function of the time, it is possible to measure the velocity of the interface, indicated with v_i.

v_i is essentially constant and equal to 0.037 ± 0.0033 cm/days for the spheres shown in *Figure 5.3 (a)* while v_i is equal to 0.032 ± 0.0045 cm/days for spheres with a diameter size of 90-125 µm. This means that the yield stress of the fluid and the volume fraction of the spheres do not play a crucial role on the compression velocity. It is rather surprising that the plastic deformation does not dominate the velocity of collapse. It does influence, however, the time at which the failure occurs (t_d).

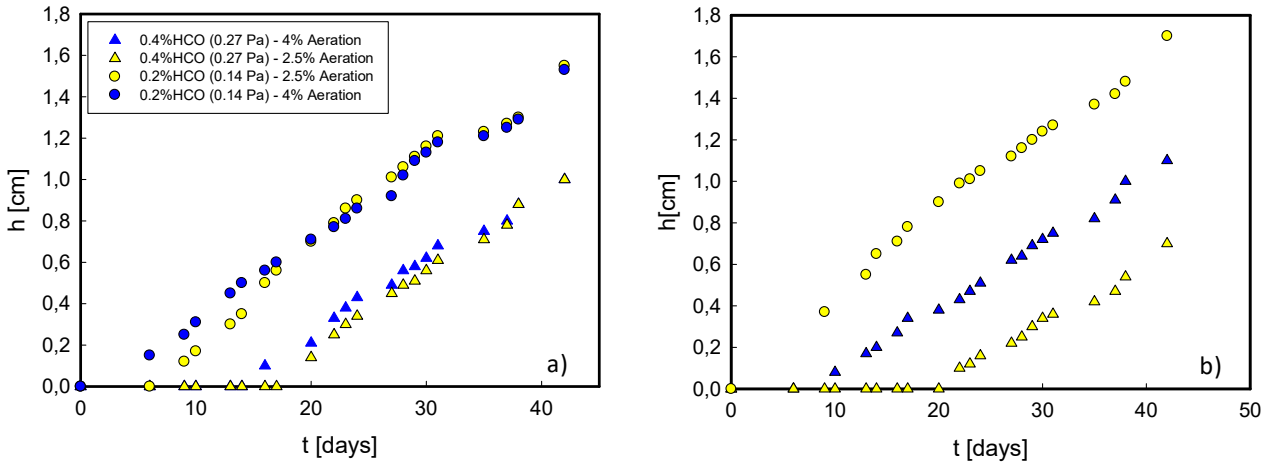

***Figure 5.3**: Splitting edge vs time in different yield stress fluids at fixed sphere sizes a) 75-90 µm ,and b) 90-125 µm*

More specifically, we can conclude from *Figure 5.3* that the time at which failure occurs strongly increases when the yield stress increases, that is by increasing HCO content. This phenomenon is more apparent in

Figure 5.4, where the temporal evolution of the height of the network at two different yield stress of the fluids (0.14 Pa and 0.21 Pa) is plotted at a fixed volume fraction for the spheres (4%). Different curves correspond to various diameters. Spheres with smaller diameter need more time

to start the gravitational collapse, so t_d is longer for the particle loads with smaller beads. It is important to highlight that

Figure 5.4 refers to beads characterized by different density values. The smallest beads have higher densities and, as such, apply a smaller load on the suspensions during their rising motion. With increasing spheres dimensions, the densities decrease and the load applied on the suspensions increases. The contribution of the sphere size is more relevant than the density mismatch, due to the fact that the size can change up to one order of magnitude.

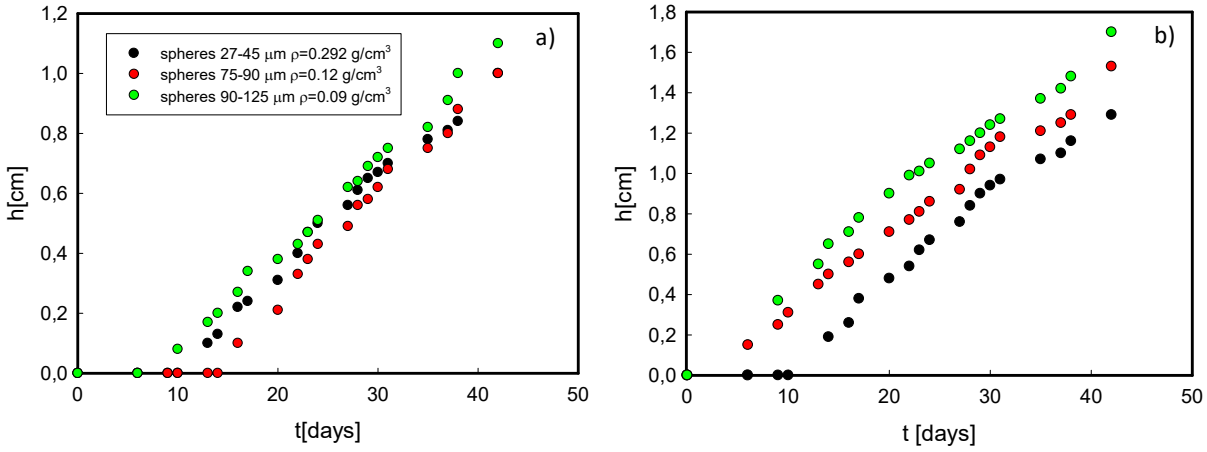

***Figure 5.4**: Splitting edge as function of the time at fixed volume fraction (4%) in different yield stress fluids: a) 0.27 Pa, b) 0.14Pa*

The range of the experimental data is not sufficient to be fitted with the Poroelastic model. It is possible to plot the delay time (t_d) at which the failure occurs as function of the volume fraction content, as shown in *Figure 5.5 (a)*. The delay time is inversely proportional to the sphere concentration and shows no systematic dependence upon particle size.

Further evidence that the yield properties of the network also determine the initial stage of compr ession can be seen in *Figure 5.5 (b)*. Indeed, at fixed bubble size, t_d is systematically larger with

increasing fiber content (i.e. yield stress of the fluid) and it is inversely proportional to the volume fraction.

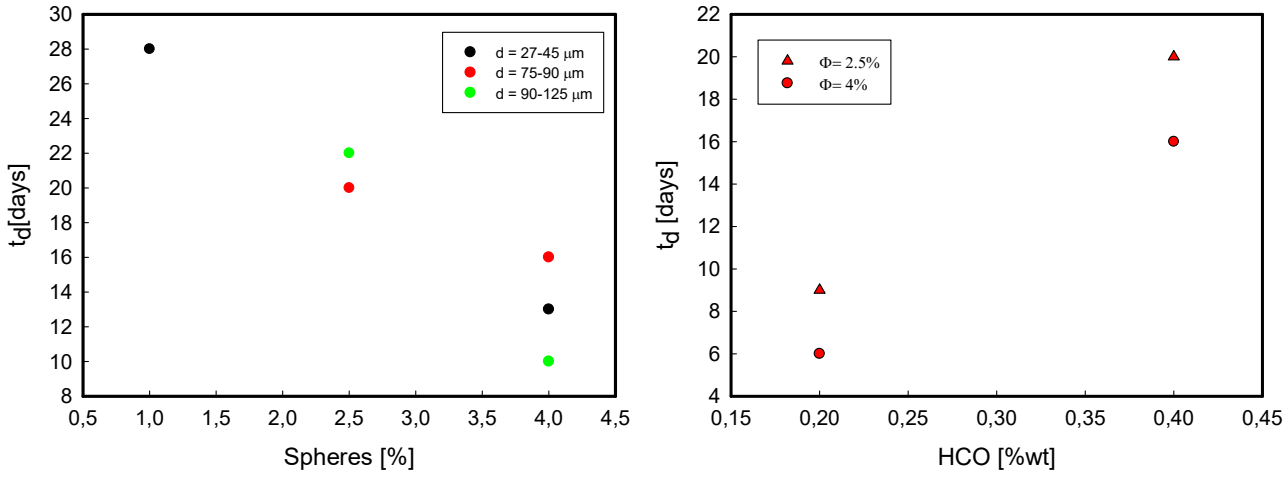

Figure 5.5**:** *a) Delay time dependence on spheres concentration at fixed yield stress fluid parametric on the bubble size b) Delay time as function of the fibers content parametric on the volume fraction at fixed bubble size (75-90 µm)*

In conclusion, the gravitational collapse of HCO - networks is described by two parameters: the velocity of the interface and the delay time at which the instability appears. The velocity of the interface does not depend significantly upon the yield stress of the fluid and of the volume fraction of the spheres but it does depend on the sphere size. The delay time is inversely proportional to the volume fraction and directly proportional to the fiber content.

5.2. Stability under air bubble load.

The effect of air bubbles on the physical stability of our structured and highly aerated samples is studied varying aeration levels at different temperatures (T=25-30-50 °C) and at different yield stress values for the fluids.

In *Figure 5.6* the values of the yield stress, extrapolated by the Herschel–Bulkley fit (as shown in Materials and Methods section), are reported as function of the fibers content, at various

temperatures.

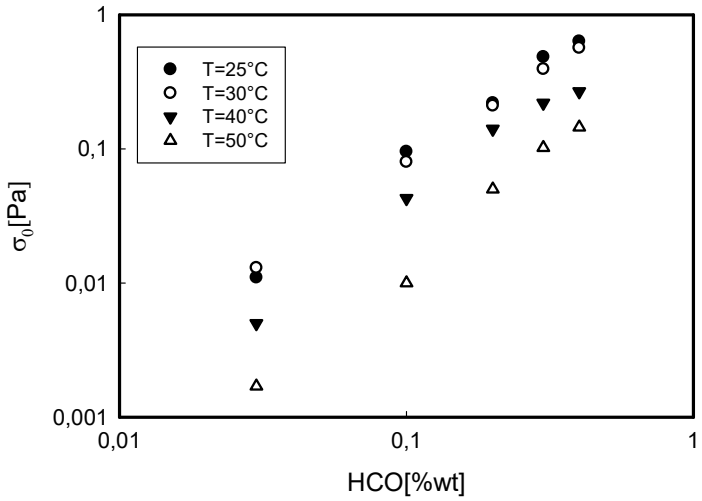

Figure 5.6:*Yield stress values at different temperatures (T=25-30-40-50°C).*

From the model prediction reported in Fig. 4.3 regarding the motion of the single body motion, it is possible to define the minimum size of the bubble able to move in the specific fluid. The values of the critical size r_c for each fluid are shown in *Table 4.*

HCO %wt	**σ_0 [Pa] T=25°C**	**r_c[µm] T=25°C**	**σ_0 [Pa] T=30°C**	**r_c[µm] T=30°C**	**σ_0 [Pa] T=40°C**	**r_c[µm] T=40°C**	**σ_0 [Pa] T=50°C**	**r_c[µm] T=50°C**
0.1	0.095	103.86	0.08	87.46	0.043	46.79	0.010	10.93
0.2	0.220	240.53	0.213	232.87	0.141	153.83	0.050	54.66
0.3	0.487	532.43	0.394	430.76	0.220	240.52	0.102	111.52
0.4	0.634	693.15	0.567	619.90	0.268	293.00	0.145	158.53

Table 4: *Yield stress values at different temperatures (25-30-40-50°C) and the respective critical radius of the bubbles.*

There are many ways to introduce stable air bubbles into a structured fluid. Of course, a choice among them can be done considering the features of the air bubble dispersion that we need to achieve. In this work, aerated samples are made with two different methods, as properly explained in the materials and methods section: by a membrane emulsification unit in a way to produce air bubbles with homogeneous diameter size and by mechanical agitation to create a non uniform bubble size distribution. As it will be explained more in details later, the bubble size polydispersity has a fundamental role on the physical instability of the studied systems. As such, we decided to separate the cases of presence of homogeneous bubble sizes produced via the emulsification unit and the heterogeneous case produced via mechanical mixing.

5.2.1 Homogeneous bubbles size

Four fluids are analyzed containing a different amount of fibers, ranging from 0.1 to 0.4 % wt. The volume fraction of the air bubbles is fixed at 1% and 3%. The diameter of the air bubbles ranges from 40 to 60 μm.

It is important to highlight that the average diameter of the produced bubbles is always smaller than the critical values shown in *Table 4* except in the case of very low HCO content (0.1%) and highest temperatures (50°C).

5.2.1.1 Loading tests

In the following, the results for the samples with HCO= [0.1%] and with an aeration level of 3% are shown. As it is possible to see from *Figure 5.7*, the samples in these conditions are not unstable. The air bubbles do not remain entrapped inside the fluid and they are free to escape from the bottom to the top. The change in the sample turbidity indicates that the air bubbles content decreases in time.

T= 25°C

T=30°C

T=50°C

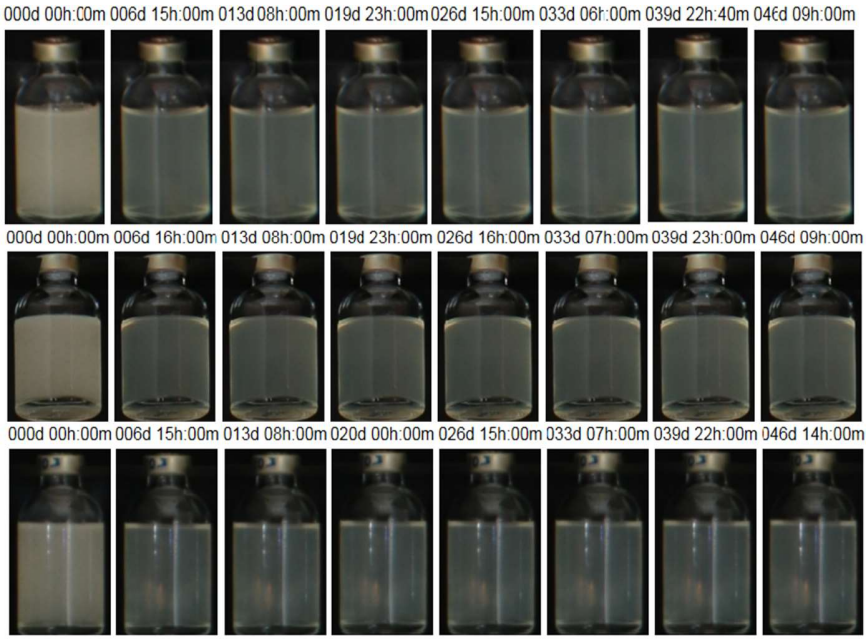

Figure 5.7: *Time Evolution of Loading Test Samples at HCO = [0.1%] at different temperatures with the initial air bubbles volume fraction equal to 3%.*

Figure 5.8 shows the pictures taken over time for the sample with HCO= [0.4%] and 3% of aeration. Under these conditions, it is possible to see the gravitational collapse effect, apparent only at 50°C, due to the increased value of the yield stress and, hence, the increased resistance exerted by the fluid to the bubble motion.

T= 25°C

T=30°C

T=50°C

Figure 5.8: *Time Evolution of Loading Test Samples at HCO = [0.4%] at different temperatures with initial air bubbles volume fraction of 3%*

It is possible to measure, as already shown with the solid spheres, the height of the splitting edge as function of time. *Figure 5.9* shows the temporal evolution of the height of the network for the pictures shown in *Figure 5.8*. It is apparent that the height changes sharply with time in the first month, and then saturates to a plateau value, very far from the total height of the liquid in the vial ($4.5 \pm 0.2cm$). From a linear regression of the first part before saturation, it is possible to calculate the slope and, as such, the rising interface velocity of the moving interface. In this case, the velocity is roughly 0.038 cm/days, similar to the interface velocity found for the hollow glass microspheres (see Chapter 5.1)

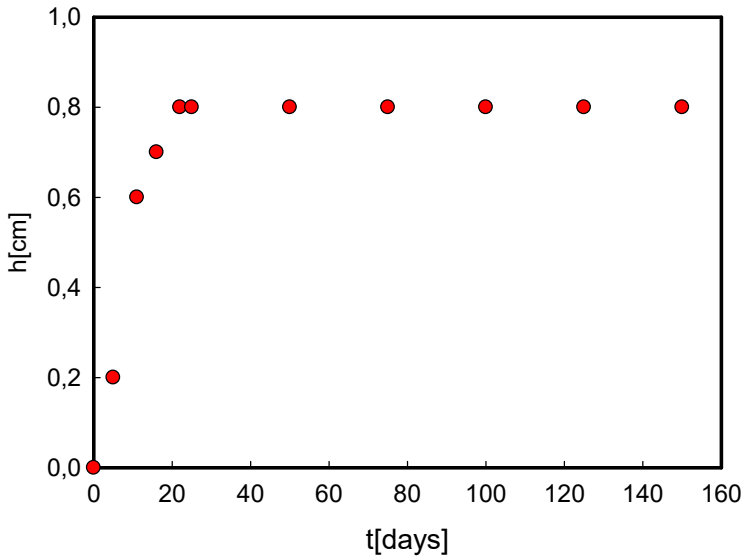

Figure 5.9: *Splitting edge versus time for the sample with HCO= [0.4%] and aeration level equal to 3%, at T=50°C.*

All the samples at T=25°C and 30°C show a physical stability behavior.

5.2.1.2 Heterogeneous bubble size

5.2.1.3 Loading tests

Forty five different samples, with fiber content from 0.2 to 0.4% wt and air bubble volume fraction ranging from 2 to 5%, are used to study the effect of air bubbles on their physical stability at different temperatures (T=25-30-50 °C). The tests were carried out for more than three months.

Samples at 25 and 30°C did not show any physical instability. *Figure 5.10* shows just one sample (with HCO= [0.4%]) at different aeration levels.

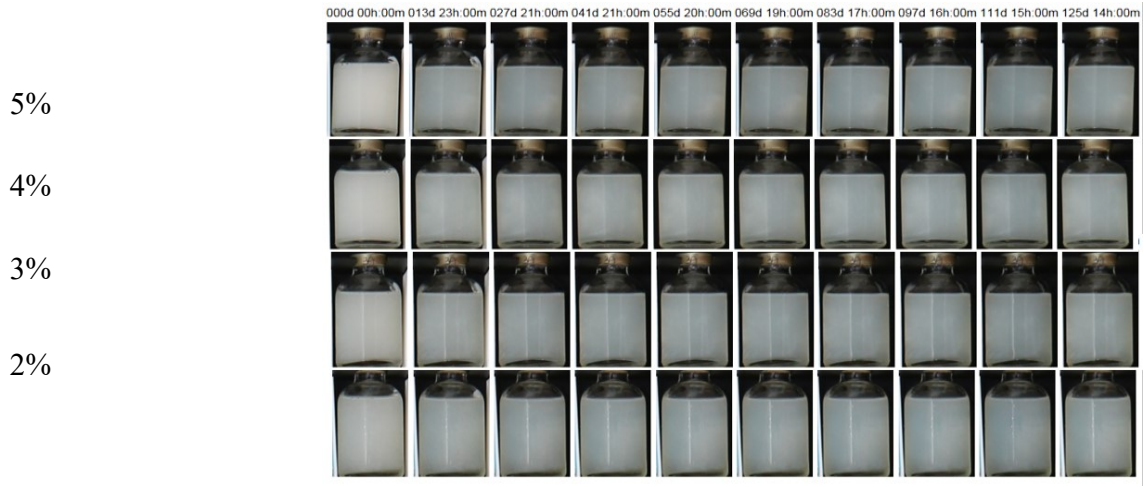

Figure 5.10: *Loading test of the sample at HCO= [0.4%] with different aeration levels (ranging from 2 to 5%) at fixed Temperature (30°C)*

At 50°C the samples with fiber content equal to 0.3% and 0.4% wt show a gravitational collapse effect, as shown in *Figure 5.11* and in *Figure 5.12*. It has to be marked that in some cases (such as the one referred to 0.3% of HCO content and 5% and 3% of aeration) a flocculation failure mode appears.

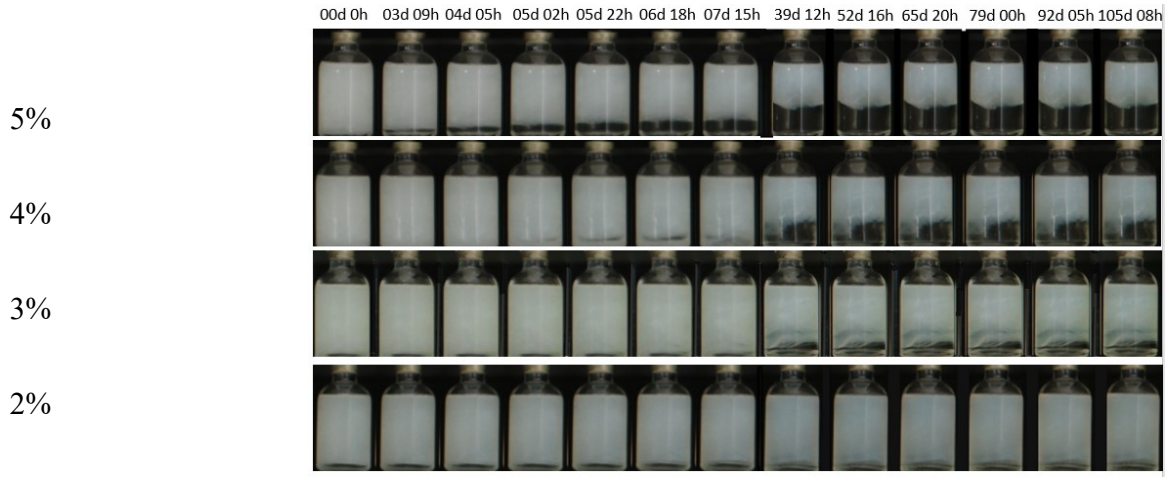

Figure 5.11: *Loading tests of the sample at HCO= [0.4%] with different aeration levels (ranging from 2 to 5%) at fixed Temperature (50°C)*

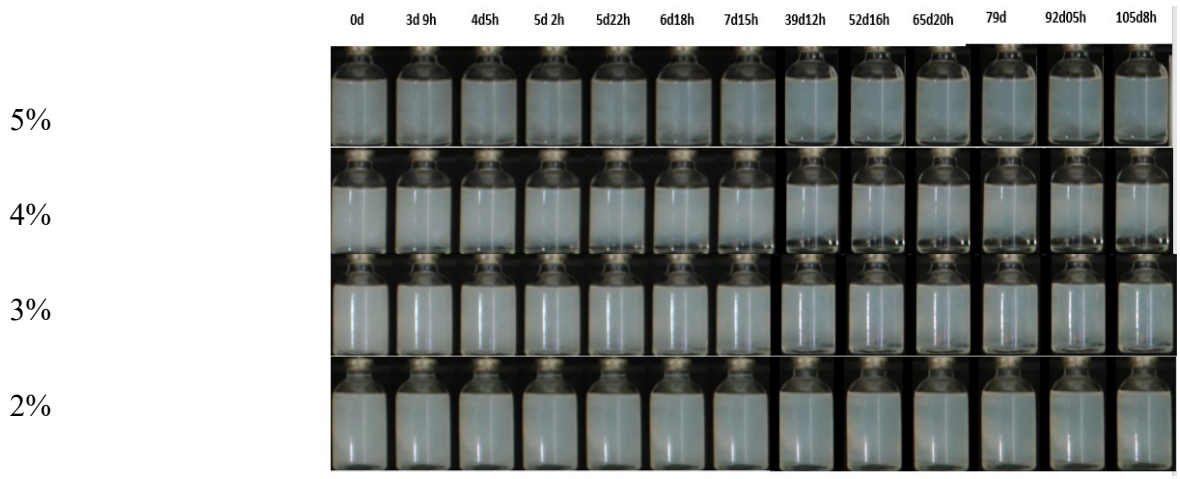

***Figure 5.12**: Loading tests of the sample at HCO= [0.3%] with different aeration levels (ranging from 2 to 5%) at fixed Temperature (30°C)*

All test results at different temperatures are shown in *Figure 5.13*, in a phase diagram where different instabilities are indicated with different colors. The collapse and flocculation effects are shown in red and yellow color, respectively; while the stability phenomenon is shown with a green symbol.

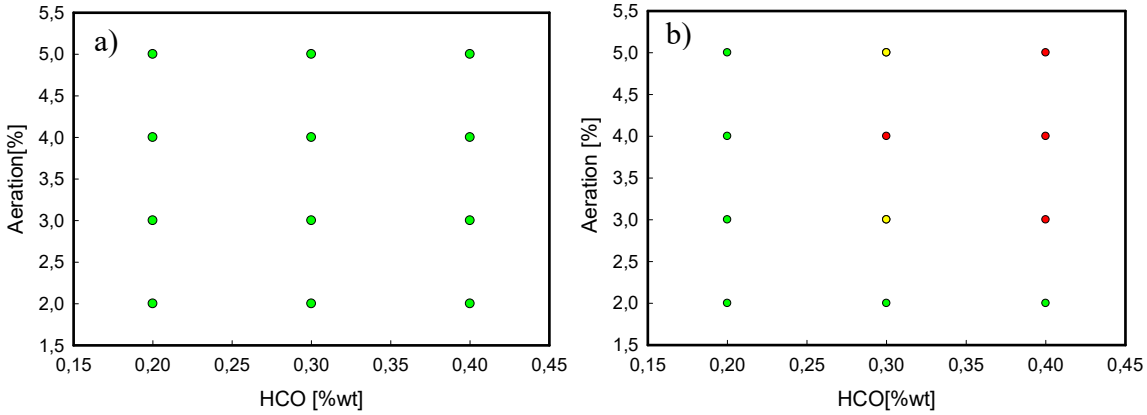

Figure 5.13: *Stability Phase diagram: yellow or red dot means that a failure occurs in the related samples (flocculation and collapse, respectively) while a green symbol indicates that the relative samples are stable. (a) T=25-30°C ; b) T=50°C.*

The aim of *Figure 5.13* is to understand if a failure occurs and which fluids are involved and, of course, to focus on the fluids that show instability to study its dynamics. Only samples with HCO= [0.3-0.4%] and aeration level higher than 3%, at 50°C, collapse. The variation of the temporal evolution of the height of the network is plotted in *Figure 5.14*. For each sample, two slopes, again, characterize the behavior of the splitting edge during time. For low times, there is a fast increase of the rising interface height with time, followed by a plateau region characterized by a specific value of the height, dependent on the aeration level. It is interesting to notice that the dynamics of the splitting edge with homogeneous (*Figure 5.9*) and heterogeneous spheres (*Figure 5.14 a*) in the same working conditions (T=50°C, 0.4% HCO and 3% aeration) is similar.

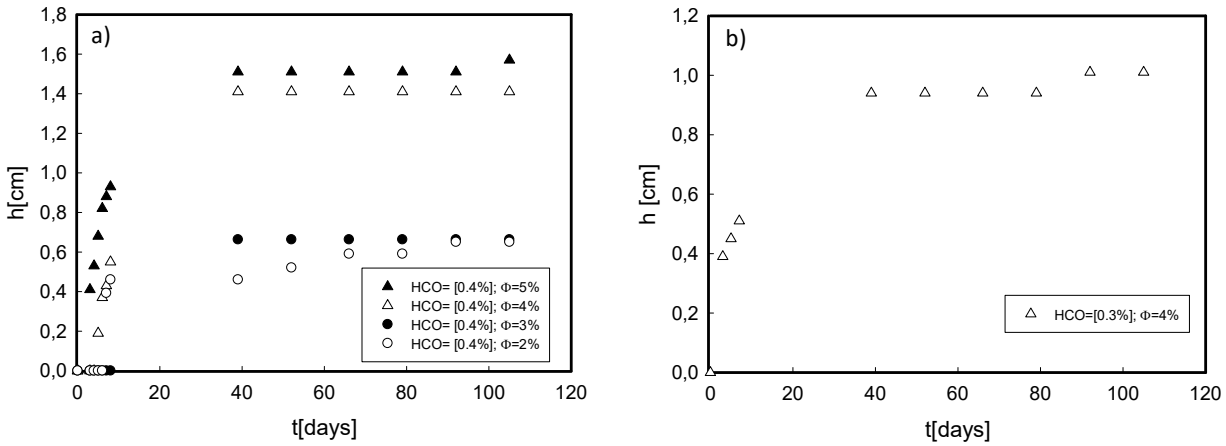

Figure 5.14: *Splitting edge as function of time at T= 50°C for: a) HCO = [0.4%] and b) HCO= [0.3%].See legend for details about the aeration level of the samples.*

Moreover, it is important to highlight that the velocity of the splitting edge is not strongly dependent on the aeration level, whereas the time at which the instability appears increases with decreasing aeration level and increasing HCO content (i.e. yield stress of the fluid). The velocity of the splitting edge is roughly 0.12 cm/days for the case with HCO = [0.4%] whereas for HCO = [0.3%] it was not possible to measure it accurately.

The poroelastic model well describes the gravitational collapse of our system. It has been applied to describe h(t) in the two stages: the initial compression and the consolidation regime. In *Figure 5.15* the behavior of the splitting edge at HCO = [0.4%] at two different aeration levels (4-5%) is reported, along with the sample at HCO = [0.3%] and 4% of aeration. The time is normalized by subtracting the delay time of each data set to the experimental time. The curves are well fitted by the Poroelastic models (black line, *Equation (*1.8*)* and the results are shown in

Table 5. The two samples at fixed fiber concentration of 0.4% show the same slope in the initial compression. A different slope is instead found for HCO= [0.3%]; this means that the initial velocity of the interface depends on the yield stress of the fluid but not on the aeration level. It is possible from *Equation 1.9* to calculate the time scale for collapse and the permeability of the

network. The values are reported in *Table 5*. The increase in gel permeability with decreasing fiber content can be justified by a larger network size.

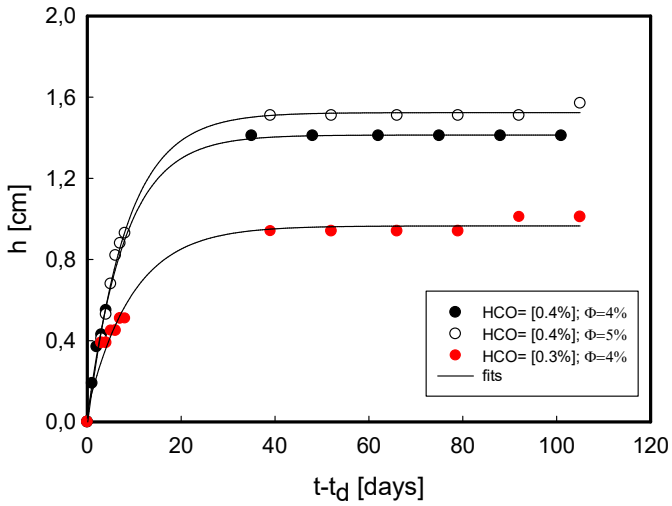

***Figure 5.15**: Splitting Edge Motion and Manley Model fit of Collapsed Samples*

Sample	k_0 (μm^2)	τ (days)
HCO=[0.4%] ϕ=5%	41	8
HCO=[0.4%] ϕ=4%	43	8
HCO=[0.3%] ϕ=4%	59	10

***Table 5**: Permeability of Collapsed Samples.*

The splitting edge trend analyzed for the air bubble loading tests is different if compared to the hollow glass microspheres, discussed in Chapter 5.1. Indeed, for the hollow glass microspheres it is not possible to visualize the plateau region of the splitting height, but only a continuous increase of the height with time. A possible explanation for this difference can be given by considering that the loading tests for the spheres are carried out for a limited period of 30 days, whereas for the air bubbles the tests are performed for more than 100 days. Of course, the dynamic of the bubbles is more complicated than the rising motion of solid spheres due to different phenomena that can appear with bubbles and not with solid spheres (such as ripening, desorption/absorption, surface deformation etc).

Also the physical stability results are different: the bubbles show collapse and flocculation phenomena only for the sample with fiber concentration above 0.3%wt; for the hollow glass microsphere a fiber content HCO = [0.2%] is already sufficient to induce an instability phenomenon.

6. Conclusions

The motion of bubbles and hollow microspheres rising in a structured fluid showing a yield stress has been analyzed. The suspending fluid is a surfactant solution containing different fiber content that can be tuned in a way to vary the yield-stress value. A deep rheological study of the fluids has been carried out and the rheological parameters have been evaluated by considering the Herschel-Bulkley constitutive equation. As the HCO content is increased, the elastic response increases and a plateau modulus at low frequency appears, indicating the fingerprint of a gel-like network. Steady flow measurements confirm this response, by showing a yield stress at low shear rate values.

Data are fitted by a power law equation where G_0 and σ_0 are proportional to C^{α}, where C is the fibers concentration. In our case, α is roughly 1.23 for both yield stress and elastic modulus. Our measurements are compared with those of Merleier *et al.* (2014) and they are in good agreement, although with a unique slope valid for the whole HCO range. By tuning the surfactant concentration, the elastic modulus has been proven to be dependent on the LAS content and the experimental results have been analyzed in terms of depletion interactions between the HCO fibers.

The rising velocity of rigid hollow spheres of different sizes and air bubbles, freely incorporated in the system during the mixing process, has been measured by tracking tests performed through a home-made time-lapse apparatus. Finite element simulations have been performed to support the experimental data. The experimental results confirm the existence of a critical diameter beyond which the spherical particle can move. As expected, such a critical size depends on the yield stress of the fluid. A comparison with numerical simulations has been carried out in terms of dimensionless variables by plotting the three fundamental characteristic numbers: the Stokes drag coefficient, the Bingham number, and the yield stress ratio. The good agreement between experiments and simulations suggests that, at least for the problem of a sphere motion and the experimental conditions adopted in this work, the structured liquids used in our experiments can be well modeled by standard constitutive equations for yield-stress fluids. The power law index *n* plays a significant role, in particular in the medium Bingham range value. This explains the difference between available data in the literature on Carbopol (well described by n=0.5) and our solutions (n approaching 1). Numerical simulations performed for different values of the power law index *n* confirmed these results. The results are well summarized in Figs. 4.2 and 4.3, which

can be used also as a valuable tool to predict the local mechanical properties of the suspending fluid at very low shear rates, often much lower than the typical sensitivity of commercial rheometers. They can be also used to discern between motion/no motion of submerged bodies in yield stress fluids and to indirectly measure their terminal velocity. Moreover, it is important to highlight that from a traditional rheological measurement, which is relatively short in time, it is possible to evaluate the terminal velocity of a sphere that, instead, would need an experimental time of several weeks. The results presented here have important implications for home-care industrial applications where many detergents show rheological properties similar to the structured fluids considered in this work.

At last, loading tests are performed at different temperatures ranging from 25°C to 50°C on highly aerated and structured fluids in order to understand the effect of air bubbles on the physical stability. Each tested formula is poured in a glass vial and the aeration level is measured before each pouring by a specific weight static measurement; at the same time, each vial is sampled in order to obtain the bubble size distribution by a macro time lapse set up. Experiments with homogeneous and heterogeneous bubble size distribution have been performed. The bubble size is far below the critical diameter for which the motion of the single bubble would take place in the specific fluid. The first result we obtain is a sort of phase diagram in which, for each value of the structurant level and effective aeration content we are able to identify the samples interested in a failure. Secondly, when a failure occurred, we had the opportunity to study its dynamics and to differentiate between collapse and flocculation. The collapse has been studied and the dynamics of the splitting edge has been reported as function of time for an experimental period of more than three months. Samples with the highest level of structurant content (high yield stress values) and with aeration levels above 2% at T= 50°C tends to collapse. The height of the moving boundary due to the incoming phase separation increases with time and then saturates at different plateaus values, depending on the initial aeration content. The time at which the collapse starts and the final plateau are strongly dependent on the yield stress of the fluid and the aeration content. The data are compared with experiments performed using hollow glass microspheres, the results are qualitatively and quantitatively different: the bubbles show collapse and flocculation phenomena only for the sample with fiber concentration above 0.3%wt; for the hollow glass microsphere a fiber content HCO = [0.2%] is already sufficient to induce an instability phenomenon. The splitting edge trend analyzed

is also different. Indeed, for the hollow glass microspheres it is not possible to visualize the plateau region of the splitting height, but only a continuous increase of the height with time. A possible explanation for this difference can be given by considering that the loading tests for the spheres are carried out for a limited period of 30 days, whereas for the air bubbles the tests are performed for more than 100 days.

7. References

- Alargova, R. G.; Warhadpande, D. S.; Paunov, V. N.; Velev, O. D. “Foam superstabilization by polymer microrods”. Langmuir, 20, 10371 (2004).
- Allain C., M. Cloitre, M. Wafra, Aggregation and sedimentation in colloidal suspensions, Phys. Rev. Lett. 74,1478–1481 (1995).
- Ansley, R. W. and Smith, T. N., “Motion of spherical particles in a Bingham plastic,” AIChE J. 13, 1193–1196, (1967).
- Astarita, G. and Apuzzo, G., “Motion of gas bubbles in non-Newtonian liquids,” AlChE J. 11, 815–820 (1965).
- Astarita, G., “The engineering reality of the yield stress,” J. Rheol., 34, 275-277 (1990).
- Atapattu, D. D., Chhabra, R. P., and Uhlherr, P. H. T., “Creeping sphere motion in Herschel-Bulkley fluids: Flow field and drag,” J. Non-Newtonian Fluid Mech. 59, 245–265 (1995).
- Ball, R. C., “Fractal colloids aggregates: consolidation and elasticity” Physica D, 38, 13, (1989).
- Balmforth, N. J., Frigaard, I. A., and Ovarlez, G., “Yielding to stress: Recent developments in viscoplastic fluid mechanics,” Annu. Rev. Fluid Mech. 46, 121–146 (2014).
- Barnes H.A.; A Handbook of Elementary Rheology, The University of Wales Institute of NonNewtonian Fluid Mechanics (2000).
- Barnes, H. A., “The yield stress—A review or ‘panta roi’—Everything flows?” J. Non-Newtonian Fluid Mech. 81, 133–178 (1999).
- Barnes, H.A, Walters, K, “The yield stress myth?” Rheol. Acta., 24 (4), 323 -326. (1985)
- Bartlett P., L. J. Teece, M. A. Faers, Sudden collapse of a colloidal gel, Phys. Rev. E 85 021404.(2012)
- Beaulne, M. and Mitsoulis, E., “Creeping motion of a sphere in tubes filled with Herschel-Bulkley fluids,” J. Non-Newtonian Fluid Mech. 72, 55–71 (1997).
- Beris, A. N., Tsamopoulos, J. A., Armstrong, R. C., and Brown, R. A., “Creeping flow of a sphere through a Bingham plastic,” J. Fluid Mech. 158, 219–244, (1985).
- Berret, J.F.o., “Rheology of wormlike micelles: equilibrium properties and shear bandi ng transitions”, in Molecular gels., Springer. p. 667-720 (2006).
- Berry G.C., "Rheological and Rheo-Optical Studies with Nematogenic Solutions of a Rodlike Polymer: A Review of Data on Poly (phenylene benzobisthiazole)", (Springer-Verlag: New York, (1987).
- Bhavaraju, S. M., Mashelkar, R. A., and Blanch, H. W., “Bubble motion and mass transfer in non-Newtonian fluids: Part I. Single bubble in power law and Bingham fluids,” AIChE J. 24, 1063–1070 (1978).

- Biot, M.A., “General theory of three dimensional consolidation. Journal of applied physics”, 12(2): p. 155-164, (1941).
- Blackery, J. and Mitsoulis, E., “Creeping motion of a sphere in tubes filled with a Bingham plastic material,” J. Non-Newtonian Fluid Mech. 70, 59–77 (1997).
- Blijdenstein T.B.J., E. van der Linden, T. van Vliet, G. A. van Aken, “Scaling behavior of delayed demixing, rheology, and microstructure of emulsions flocculated by depletion and bridging”, Langmuir 20,11321–11328. 9 (2004).
- Brinke A. J. W. ten, L. Bailey, H. N. W. Lekkerkerker and G. C. Maitland, “Rheology modification in mixed shape colloidal dispersions. Part I: pure components”, Soft Matter, 3, 1145–1162, (2007).
- Brown, W. D.,”The structure and physical properties of flocculation colloids”, PhD thesis, University of Cambridge, Cambridge, U.K., (1987).
- Brown, W. D.; Ball, “Computer simulation of chemically limited aggregation”,R. C. J. Phys. A , 18, L517, (1985).
- Buscall R., Choudhury T, Faers M, Goodwin J, de Paul A., Luckham P. and Partridge S, “Towards rationalising collapse times for the delayed sedimentation of weakly-aggregated colloidal gels”, Soft Matter, Issue 7, (2009).
- Buscall, R. and L.R. White, “The consolidation of concentrated suspensions. Part 1. The theory of sedimentation”. J. Chem. Soc., Faraday Trans. 1, **83**(3): p. 873-891, (1987).
- Buscall, R.; Mills, P. D. A.; Goodwin, J. W.; Lawson, D. W., “Scaling Behaviour of the Rheology of Aggregate Networks formed from Colloidal Particles” J. Chem. Soc., Faraday Trans. 1, 84, 4249, (1988).
- Caggioni, M., P. Hogben, and F. Luo, “Shampoo stability, theoretical framework to model degradation and failure modes.” P&G Smart Learning Report, (2012).
- Cates, M.E. and S.J. Candau, “Statics and dynamics of wormlike surfactant micelles.” Journ al of Physics: Condensed Matter, 2(33): p. 6869.(1990)
- Chafe, N. P. and de Bruyn, J. R., “Drag and relaxation in a bentonite clay suspension,” J. Non-Newtonian Fluid Mech. 131, 44–52 (2005).
- Chan Man Fong C.M, C.F., De Kee, D. and Gryte C.J. Non Newtonian fluid Mech., 46,111 (1993)
- Chen Y.-L. and K. S. Schweizer, “Depletion interactions in suspensions of spheres and rod–polymers”,Journal of chemical physics 3, 117, 2002.
- Clift, R., Grace, J. R., and Weber, M. E., Bubbles, Drops and Particles (Academic Press, New York, 1978).
- D’Avino, G., Tuccillo, T., Maffettone, P. L., Greco, F., and Hulsen, M. A., “Numerical simulations of particle migration in a viscoelastic fluid subjected to shear flow,” Comput. Fluids 39, 709–721 (2010).

- de Bruyn, J. R., “Age dependence of the drag force in an aqueous foam,” Rheol. Acta 45, 803–811 (2006).
- de Bruyn, J. R., “Transient and steady-state drag in foam,” Rheol. Acta 44, 150–159 (2004).
- De Gennes P.-G., “Scaling concepts in polymer physics”, Cornell University Press, (1979).
- De Meirleir N., Pellens L., Broeckx W, van Assche G., De Malsche W., “The rheological properties of hydrogenated castor oil crystals” Colloid Polym Sci, 292,2539–2547 (2014).
- Deglo de Besses, B., Magnin, A., and Jay, P., “Sphere drag in a viscoplastic fluid,” AIChE J. 50, 2627–2629 (2004).
- Denkov, N. D., Subramanian, V., Gurovich, D., and Lips, A., “Wall slip and viscous dissipation in sheared foams: Effect of surface mobility,” Colloids Surf., A 263, 129–145 (2005).
- Denkov, N. D., Tcholakova, S., Golemanov, K., Ananthpadmanabhan, K. P., and Lips, A., “The role of surfactant type and bubble surface mobility in foam rheology,” Soft Matter 5, 3389–3408 (2009).
- Derec C., D. Senis, L. Talini, C. Allain, “Rapid settling of a colloidal gel”, Phys. Rev. E 67,062401 (2003)
- Derksen, P. J. J., “Direct simulations of spherical particle motion in Bingham liquids,” Comput. Chem. Eng. 35, 1200–1214 (2011).
- Dezhi, G. and Tanner, R. I., “The drag on a sphere in a power-law fluid,” J. Non-Newtonian Fluid Mech. 17, 1–12 (1985).
- Dhont J. K. G. and W. J. Briels, “Viscoelasticity of suspensions of long, rigid rods”,Colloids Surf., A, 213, 131– 156, (2003).
- Dimakopoulos, Y., Pavlidis, M., and Tsamopoulos, J., “Steady bubble rise in Herschel-Bulkley fluids and comparision of predictions via the augmented Lagrangian method with those via the Papanastasiou model,” J. Non-Newtonian Fluid Mech. 200, 34–51 (2013).
- Doi M. and S. F. Edwards, “The Theory of Polymer Dynamics”, Clarendon Press, Oxford, (1986).
- Doi M., Edwards, “Dynamics of rod-like macromolecules in concentrated solution”. S. F. J. Chem. SOC., Faraday Trans. 2, 74, 918-932, (1978).
- Dreiss, C.A., “Wormlike micelles: where do we stand? Recent developments, linear rheology and scattering techniques”. Soft Matter, 3(8): p. 956-970 (2007).
- Dubash, N. and Frigaard, I. A., “Conditions for static bubbles in viscoplastic fluids,” Phys. Fluids 16, 4319–4330 (2004).
- Dubash, N. and Frigaard, I. A., “Propagation and stopping of air bubbles in Carbopol solutions,” J. Non-Newtonian Fluid Mech. 142, 123–134 (2007).
- Ducloue, L., Pitois, O., Goyon, J., Chateau, X., and Ovarlez, G., “Rheological ´ behavior of suspensions of bubbles in yield stress fluid,” J. Non-Newtonian Fluid Mech. 215, 31–39 (2015).

- Durian, D. J.; Weitz, D. A.; Pine, D. J. Scaling behavior in shaving cream. Phys. Rev. A, 44, R7902.(1991)
- Emady, H., Caggioni, M., and Spicer, P., "Colloidal microstructure effects on particle sedimentation in yield stress fluids," J. Rheol. 57, 1761 (2013).
- Evans R. M. L and Starrs L., J. Phys. Condens. Matter 14, 2507 (2002).
- Fraggedakis, D., Dimakopoulos, Y., and Tsamopoulos, J., "Yielding the yieldstress analysis: A study focused on the effects of elasticity on the settling of a single spherical particle in simple yield-stress fluids," Soft Matter 12, 5378–5401 (2016a).
- Fraggedakis, D., Pavlidis, M., Dimakopoulos, Y., and Tsamopoulos, J., "On the velocity discontinuity at a critical volume of a bubble rising in a viscoelastic fluid," J. Fluid Mech. 789, 310–346 (2016b).
- Gaudino D., R. Pasquino, and N. Grizzuti, " Adding salt to a surfactant solution: Linear rheological response of the resulting morphologies" Journal of Rheology 59, 1363 (2015);
- Glasrud G.G., R. C. Navarrete, L. E. Scriven, C. W. Macosko, "Settling behaviors of iron-oxide suspensions", AIChE Journal 39, 560–568 (1993).
- Gonzenbach, U. T.; Studart, A. R.; Tervoort, E.; Gauckler, L. J. "Stabilization of foams with inorganic colloidal particles". Langmuir , 22, 10983.(2006)
- Gopalakrishnan V., K. S. Schweizer, C. F. Zukoski, "Linking single particle rearrangements to delayed collapse times in transient depletion gels", J. Phys.: Condens. Matter 18 11531–11550 (2006)
- Gueslin, B., Talini, L., Herzhaft, B., Peysson, Y., and Allain, C., "Flow induced by a spheres settling in an aging yield stress fluid," Phys. Fluids 18, 103101 (2006).
- Harper, J. F., "The motion of bubbles and drops through liquids," Adv. Appl. Mech. 12, 59–129 (1972).
- Hong L, Anthony SM, Granick S. "Rotation in suspension of a rod-shaped colloid". Langmuir 22(17), 7128-31, (2006).
- Huang Y. Y., S. V. Ahir and E. M. Terentjev, "Dispersion rheology of carbon nanotubes in a polymer matrix".,Phys. Rev. B: Condens. Matter, 73, 125422–125421, (2006)
- Huh J.H. , M. L. Lynch, E. M. Furst, "Microscopic structure and collapse of depletion-induced gels in vesicle-polymer mixtures", Phys. Rev. E 76 (5) 051409, (2007)
- Israelachvili, J. N., D. J. Mitchell, and B. W. Ninham, "Theory of self-assembly of hydrocarbon amphiphiles," J. Chem. Soc., Faraday Trans. II 72, 1525–15, (1976).
- James, A.E., Williams, D.J.A. & Williams, P.R. "Direct measurement of static yield properties of cohesive suspensions", Rheol. Acta, 26, 437–446 (1987).
- Jossic, L. and Magnin, A., "Drag and stability of objects in a yield stress fluid," AIChE J. 47, 2666–2672 (2001).
- Kamp S. W., M. L. Kilfoil, Universal behaviour in the mechanical properties of weakly aggregated colloidal particles, Soft Matter 5, 2438–2447, (2009).

- Kamp Stephen W. Kilfoil and Maria L.,"Universal behaviour in the mechanical properties of weakly aggregated colloidal particles", Soft Matter,(2009).
- Kantor, Y.; Webman, "Elastic Properties of Random Percolating Systems" , I. Phys. Rev. Lett. 1984, 52, (1891).
- Kefi S., J. Lee, T. Pope, P. Sullivan, E. Nelson, A. Hernandez, T. Olsen, M. Parlar, B. Powers, A. Roy, A. Wilson and A. Twynam, "Expanding applications for viscoelastic surfactants"Oilfield Rev., 16, 10, (2004).
- Kerekes RJ, Soszynski RM, Tam Doo PA, "Papermaking Raw Materials", Punton V ed Mechanical Engineering Publications Limited, London, p265.(1985).
- Kilfoil M. L., E. R. Pashovski, J. A. Masters, D. A. Weitz, "Dynamics of weakly aggregated colloidal particles", Phil. Trans. R. Soc. Lond. A 361, 753–766, (2003)
- Krall A. H. and D. A. Weitz, "Internal dynamics and elasticity of fractal colloidal gels", Phys. Rev. Lett.,80, 778–781,(1998).
- Kuo-Yann Lai, "Liquid Detergents", (Taylor & Francis Group), (2015).
- Larson R.G., "The Structure and Rheology of Complex Fluids", Oxford University Press, New York, (1999).
- Larson, R.G, "The Structure and Rheology of Complex Fluids", Oxford University Press, New York ,(1999)
- Liu, B. T., Muller, S., and Denn, M. M., "Interactions of two rigid spheres translating collinearly in creeping flow in a Bingham material," J. NonNewtonian Fluid Mech. 113, 49–67 , (2003).
- Luo, H. and Pozrikidis, C., "Effect of surface slip on Stokes flow past a spherical particle in infinite fluid and near a plane wall," J. Eng. Math. 62, 1–21,(2008).
- Magnaudet, J. and Eames, I., "The motion of high-Reynolds number bubbles in inhomogeneous flows," Annu. Rev. Fluid Mech. 32, 659–708,(2000).
- Manley S., Cipelletti , V Trappe , A E Bmanleailey , R J Christianson , U Gasser , V Prasad , P N Segre , M P Doherty , S Sankaran , A L Jankovsky , B Shiley , J Bowen , J Eggers , C Kurta , T Lorik , D A Weitz Phys. Rev. Lett. 93, 108302,(2004).
- Manley S., J. M. Skotheim, L. Mahadevan, and D. A. Weitz ," Gravitational Collapse of Colloidal Gels" Physical Review Letters, 94, 218302,(2005).
- Martinez, A. C.; Rio, E.; Delon, G.; Saint-Jalmes, A.; Langevin, D.; Binks, B. P. "On the origin of the remarkable stability of aqueous foams stabilised by nanoparticles: Link with microscopic surface properties". Soft Matter 4, 1531.(2008)
- Merkak, O., Jossic, L., and Magnin, A., "Spheres and interactions between spheres moving at very low velocities in a yield stress fluid," J. NonNewtonian Fluid Mech. 133, 99–108, (2006).
- Mirzaagha S., Pasquino R., Iuliano E., D'Avino G., Zonfrilli F., Guida V, Grizzuti N., The rising motion of spheres in structured fluids with yield stress.Physics of Fluids 29, 093101 (2017)

- Mitsoulis, E. and Galazoulas, S., “Simulation of viscoplastic flow past cylinders in tubes,” J. Non-Newtonian Fluid Mech. 158, 132–141,(2009).
- Mitsoulis, E. and Tsamopoulos, J., “Numerical simulations of complex yieldstress fluid flows,” Rheol. Acta 56, 231–258,(2017).
- Mitsoulis, E., “Flows of viscoplastic materials: Models and computations,” Rheol. Rev., 135–178, (2007)
- Mitsoulis, E., “On creeping drag flow of a viscoplastic fluid past a circular cylinder: Wall effects,” Chem. Eng. Sci. 59, 789–800 ,(2004).
- Mohraz A. and M. J. Solomon, “Gelation and internal dynamics of colloidal rod aggregates”, J. Colloid Interface Sci., 300,155–162, (2006).
- Mujumdar A., Beris A. N., and Metzner A. B. “Transient phenomena in thixotropic system”s. J. Non-Newtonian Fluid Mech., 102:157-178, (2002).
- Mukhijaa D. and M. J. Solomon, "Nematic order in suspensions of colloidal rods by application of a centrifugal field", Soft Matter, 2, (2011).
- Mullineux, G., “Non-linear least squares fitting of coefficients in the Herschel– Bulkley model,” Appl. Math. Modell. 32, 2538–2551,(2008).
- Naderi A., T. Lindstro ¨m and T. Pettersson, “Carboxymethylated nanofibrillated cellulose: rheological studies”, Cellulose, 2014, 21, 2357–2368.,(2014).
- Pa¨a¨kko¨ M, Ankerfors M, Kosonen H, Nyka ¨nen A, Ahola S, O ¨sterbergM, RuokolainenJ, LaineJ, LarssonPT, IkkalaO, Lindstro¨mT. “Enzymatic hydrolysis combined with mechanical shearing and high-pressure homogenization for nanoscale cellulose fibrils and strong gels.” Biomacromolecules 8(6):1934–1941, (2007).
- Packman M.K. and Th.F. Tadros , “Depletion flocculation of concentrated latex suspensions by surfactant micelles”, Colloids and surfaces Volume 67, IssueC,(1992).
- Papanastasiou, T. C., “Flows of materials with yield,” J. Rheol. 31, 385–404 (1987). Procter & Gamble, EP01396535B1 patent 02447167.4 (2004).
- Parker A., P. A. Gunning, K. Ng, M. M. Robins, “How does Xanthan stabilize salad dressing?, Food Hydrocolloid “9 , 333–342, (1995).
- Pasquino R., M. Di Domenico, F. Izzo, D. Gaudino, V. Vanzanella, N. Grizzuti and B. de Gennaro,”Rheology-sensitive response of zeolite-supported anti-inflammatory drug systems”, Colloids Surf., B, 146, 938, (2016).
- Petrie C. J. S., Petrie, C. J. S. , “The rheology of fibre suspensions,” J. Non-Newtonian Fluid Mech., 87, 369–402, (1999)
- Poon W. C. K., L. Starrs, S. P. Meeker, A. Moussaid, R. M. L. Evans, P. N. Pusey, M. M. Robins, “Delayed sedimentation of transient gels in colloidpolymer mixtures: Dark-field observation, rheology and dynamic light scattering studies”, Faraday Discuss. 112,143–154. (1999)

- Poon, W.C.K., “The physics of a model colloidpolymer mixture”. Journal of Physics: Conde nsed Matter, 14 (33) (2002).
- Powell R.L., “Rheology of suspensions of rodlike particles”, J. Stat. Phys., 62, 1073–1094, (1991).
- Procter & Gamble, EP01396535B1, Patent No: 02447167.4, (2004).
- Pryamitsyn V. and V. Ganesan, “Screening of hydrodynamic interactions in Brownian rod suspensions.”, J. Chem. Phys., 128, 134901, (2008).
- Putz, A. M. V., Burghelea, T. I., Frigaard, I. A., and Martinez, D. M., “Settling of an isolated spherical particle in a yield stress shear thinning fluid,” Phys. Fluids 20, 033102–033111 (2008).
- Quennouz N., Sara M. Hashmi,Hong Sung Choi, Jin Woong Kimcd and Chinedum O. Osuji “Rheology of cellulose nanofibrils in the presence of surfactants”, Soft Matter,12,157-164, (2016).
- Rahnama M., D. L. Koch and E. S. G. Shaqfeh, “The effect of hydrodynamic interactions on the orientation distribution in a fiber suspension subject to simple shear flow,” Phys. Fluids, 7, 487–506, (1995).
- Reiner M.,”The Deborah number”. Physics Today 17, 62. (1964).
- Rezayati Charani P, Dehghani-Firouzabadi M, Afra E, Shakeri A “Rheological characterization of high concentrated MFC gel from kenaf unbleached pulp”. Cellulose 20(2):727–740.(2013)
- Roquet, N. and Saramito, P., “An adaptive finite element method for Bingham fluid flows around a cylinder,” Comput. Methods Appl. Mech. Eng. 192, 3317–3341 (2003).
- Russo P.S., “Dynamic Light Scattering: The Method and Some Applications”, (Oxford University Press, Oxford, pp. 512–553, (1995).
- Saint-Jalmes, A. “Physical chemistry in foam drainage and coarsening.” Soft Matter, 2, 836, (2006)
- Saint-Jalmes, A.; Peugeot, M.-L.; Ferraz, H.; Langevin, D. Differences between protein and surfactant foams: Microscopic properties, stability and coarsening. Colloids Surf., A, 263, 219. (2005)
- Saito T, Uematsu T, Kimura S, Enomae T, Isogai A “Selfaligned integration of native cellulose nanofibrils towards producing diverse bulk materials.” Soft Matter 7(19): 8804–8809, (2011)
- Saramito, P. and Wachs, A., “Progress in numerical simulation of yield stress fluid flows,” Rheol. Acta 56, 211–230 (2017).
- Savenko S.V, Dijkstra M., "Phase behavior of a suspension of colloidal hard rods and nonadsorbing polymer", J Chem Phys.,124 (23), (2006).
- Senis D, Allain C, “ Scaling analysis of sediment equilibrium in aggregated colloidal suspensions”. Phys Rev E 55:7797–7800, (1997).

- Shaqfeh E. S. G and G. H. Fredrickson, “The hydrodynamic stress in a suspension of rods”, Phys. Fluids A, 2, 7– 24, (1990).
- Sherwood J. D., “The primary electroviscous effect in a suspension of rods” J. Fluid Mech., 111, 347–366 (1981).
- Sikorski, D., Tabuteaua, H., and de Bruyna, J. R., “Motion and shape of bubbles rising through a yield-stress fluid, J. Non-Newtonian Fluid Mech. 159, 10–16 (2009).
- Sober D.L., J. Y. Walz, “Measurement of Long Range Depletion Energies between a Colloidal Particle and a Flat Surface in Micellar Solutions”, Langmuir,11, 2352-2356 (29), (1995).
- Solomon M.J. and Patrick T. Spicer, “Microstructural regimes of colloidal rod suspensions, gels, and glasses”, Soft Matter, 6, 1391-1400 (2010).
- Spaans, R.D, Williams, M.C, “At last, a true liquid-phase yield stress”, J. Rheol. 39, 241–246, (1995).
- Starrs L., W. C. K. Poon, D. Hibberd, M. Robins, Collapse of transient gels in colloid-polymer mixtures, J. Phys.: Condens. Matter 14,2485–2509, (2002).
- Stover C.A., D. L. Koch and C. Cohen, “Observation of fiber orientation in simple shear flow of a semi-dilute suspension”, J. Fluid Mech.,238, 277–296, (1992).
- Tabuteau, H., Coussot, P., and de Bruyn, J., “Drag force on a sphere in steady motion through a yield-stress fluid,” J. Rheol. 51, 125–137 (2006).
- Tassieri Manlio, “Dynamics of Semiflexible Polymer Solutions in the Tightly Entangled Concentration Regime, Manlio Tassieri, Macromolecules”, 50 (14), pp 5611–5618, (2017).
- Tatsumi D, Ishioka S, Matsumoto T “Effect of fiber concentration and axial ratio on the rheological properties of cellulose fiber suspensions”. J Soc Rheol Jpn 30:27–32 (2002)
- Tcholakova, S., Denkov, N. D., Golemanov, K., Ananthapadmanabhan, K. P., and Lips, A., “Theoretical model of viscous friction inside steadily sheared foams and concentrated emulsions,” Phys. Rev. E 78, 011405–011452 (2008).
- Teece L. J., Hart J M , Hsua, K. Y, Gilligana S., M. A. Faers , P. Bartlett, “Gels under stress: The origins of delayed collapse”. Colloids and Surfaces A: Physicochem. Eng. Aspects 458, 126–133, (2014)
- Tsamopoulos, J., Dimakopoulos, Y., Chatzidai, N., Karapetsas, G., and Pavlidis, M., “Steady bubble rise and deformation in Newtonian and viscoplastic fluids and conditions for bubble entrapment,” J. Fluid Mech. 601, 123–164 (2008).
- Venerus D.C, Diffusion-induced bubble growth and collapse in yield stress fluids, J. Non-Newt. Fluid Mech. 215, 53–59, (2015)
- Verhaegh N A M, Asnaghi D and Lekkerkerker H N W “Transient gels in colloid-polymer mixtures studied with fluorescence confocal scanning laser microscopy” Physica A 264 64-74(1999).

- Weeks J. R, Duijneveldt J. S. v, and Vincent B., “Formation and collapse of gels of sterically stabilized colloidal particles”,J. Phys. Condens. Matter 12, 9599 (2000).
- Wei-Heng Shih, Wan Y Shih, Seong-Il Kim, Jun Liu, and Ilhan A Aksay, “Scaling behavior of the elastic properties of colloidal gels”. Physical Review A, 42(8):4772, (1990).
- Wilkins G. M. H., P. T. Spicer and M. J. Solomon, “Colloidal System To Explore Structural and Dynamical Transitions in Rod Networks, Gels, and Glasses”, Langmuir, 25, 8951–8959, (2009).
- Wu H,M. Morbidelli “A model relating structure of colloidal gels to their elastic properties. Langmuir 17,1030–1036 (2001).
- Yang D., A. N. Hrymak, “Rheology of Aqueous Dispersions of Hydrogenated Castor Oil”, Appl. Rheol. 23,23622,(2013).
- Yu, Z. and Wachs, A., “A fictitious domain method for dynamic simulation of particle sedimentation in Bingham fluids,” J. Non-Newtonian Fluid Mech. 145, 78–91 (2007).
- Zana R. and E. Kaler, “Giant Micelles-Properties and Applications”, (CRC, Florida), (2007).
- Zanchetta G., Mahmoudi N., Trappe V., Guida V. "Liquid detergents physical stability modeling", Final Report Procter & Gamble. (2013)
- Zhang Z.K., N. Krishna, M. P. Lettinga, J. Vermant and E. Grelet, “Reversible Gelation of Rod-Like Viruses Grafted with Thermoresponsive Polymers”, Langmuir, 25, 2437–2442, (2009).